Potential Impacts of Energy and Vehicle Transformation through 2050 on the Atmospheric Environment of Japan: focus on $PM_{2.5}$ Metals and Aerosol Acidity inducing Respiratory Inflammation

Satoko Kayaba[1,2] and Mizuo Kajino[2,3]

[1]Graduate School of Science and Technology, University of Tsukuba, Tsukuba, Ibaraki 305-8572, Japan

[2]Meteorological Research Institute, Japan Meteorological Agency, Tsukuba, Ibaraki 305-0052, Japan

[3]Faculty of Life and Environmental Sciences, University of Tsukuba, Tsukuba, Ibaraki 305-8572, Japan

Corresponding author: Satoko KAYABA (satoko@mri-jma.go.jp)

Key Points:

- Vehicle electrification effectively reduced the concentrations of Fe and Cu, which are toxic to respiratory inflammation, in $PM_{2.5}$.
- The lightweighting of battery electric vehicles reduced all non-exhaust PM from tire, brake, road wear, and resuspension.
- Changes in aerosol acidity due to gaseous pollutants reduction had little effect on the water-solubility of metals.

Abstract

The impacts of renewable energy shifting, passenger car electrification, and lightweighting through 2050 on the atmospheric concentrations of $PM_{2.5}$ total mass, Fe, Cu, and Zn, and aerosol acidity in Japan were evaluated using a regional meteorology–chemistry model. We focus on the changes in on-road exhaust/non-exhaust and upstream emissions. The domestic primary emissions of $PM_{2.5}$, Fe, Cu, and Zn were reduced by 9%, 19%, 18%, and 10%, and their surface concentrations in the urban area decreased by 8%, 13%, 18%, and 5%, respectively. On a $PM_{2.5}$ mass basis, battery electric vehicles (BEVs) have been considered to have no advantage in non-exhaust PM emissions because the increased tire and road wear and resuspension due to their heavy weight offset the benefit of brake wear reduction by regenerative brake. Indeed, passenger car electrification without lightweighting also did not significantly reduce $PM_{2.5}$ concentration in urban area in this study (−2%) but was highly effective in reducing Fe and Cu concentrations owing to their high brake wear dependence (−8% and −13%, respectively). Furthermore, the lightweigting of the drive battery and the body frame of BEVs reduced even tire and road wear and resuspension. Therefore, vehicle electrification and lightweighting could effectively reduce the risks of respiratory inflammation. The reduction of SO_x, NO_x, and NH_3 emissions changed aerosol acidity in urban area (maximum pH ±0.2). However, changes in aerosol acidity only slightly changed water-soluble metal concentrations (maximum +2% for Fe and +0.5% for Cu and Zn); therefore, it is important to focus on reducing primary metal emissions.

Plain Language Summary

Water-soluble transition metals in $PM_{2.5}$ are redox active and induce respiratory inflammation. Gaseous pollutants increase the aerosol acidity and contribute to metal dissolution and hence redox activation. In this study, the effects of renewable energy shifting, passenger car electrification, and lightweighting by 2050 on the atmospheric concentrations of $PM_{2.5}$ total mass, Fe, Cu, and Zn and aerosol acidity in Japan were evaluated using atmospheric simulation. Since the regenerative braking systems of battery electric vehicles (BEVs) have lower brake wear emissions than those of conventional vehicles, the penetration of BEVs was effective in reducing the concentrations of Fe and Cu, which have high brake wear dependence (−13% and −18%, respectively, in urban area). Current BEVs increase tire and road wear and resuspension-derived PM emissions due to their heavy weight, which can be avoided by lightweighting technologies through 2050. The reduction of gaseous pollutants from thermal power plants and on-road slightly changed aerosol acidity, but the effect on water-soluble metal concentrations was small. Therefore, it was suggested that reducing primary metal emissions is more important than gaseous pollutants in decreasing concentration of water-soluble metals that are harmful to the respiratory system, and that vehicle electrification and lightweighting are effective means for that.

1. Introduction

There is a strong association between the dry mass of particulate matter with a diameter of 2.5 μm or less ($PM_{2.5}$) and the development of cardiovascular and respiratory diseases (e.g. Pope and Dockery, 2006; Valavanidis et al., 2008). Among the various PM components, transition metals and quinones possess redox activity and are catalytically active in promoting reactive oxidation species (ROS), such as O_2^-, H_2O_2, HO_2, and OH in the body, inducing oxidative stress (e.g. Lakey et al., 2016; Shiraiwa et al., 2017; Bates et al., 2019). Kumagai et al. (2002) demonstrated that 9,10-phenanthraquinone, which has redox activity, effectively catalyzes the electron transfer from dithiothreitol (DTT) to oxygen and generates superoxide. Since then, the DTT assay has been widely used as a cell-free measure of the oxidative potential of particles. Among the metal components, Cu and Fe are especially important. Cu has the highest OP_{DTT} (the rate of DTT consumption per unit time) among transition metals. Charrier and Anastasio (2012) measured the OP_{DTT} of 10 soluble transition metals and 7 quinones and concluded that Cu(II) contributes to approximately 50% of the total DTT consumption on a typical urban air concentration basis. Fe(II) and Fe(III) substantially produce OH, the most oxidizing and toxic of the ROS, through Fenton reactions in the body (Gutteridge, 1995; Valavanidis et al., 2000; 2008; Charrier and Anastasio, 2011). OP_{DTT} is only correlated with H_2O_2 production associated with antioxidant consumption and not with OH production (Xiong et al., 2017; Jiang et al., 2019). Therefore, although the toxicity of Fe cannot be evaluated only by the OP_{DTT} index, but Fe is important in inducing oxidative stress. It is necessary that the transition metals be solubilized for them to have redox activity. Increased aerosol acidity due to sulfuric and nitric acids and the formation of metal–ligand complexes with organic matters affect metal solubility (Meskhidze et al., 2003; Oakes et al., 2012; Paris and Desboeufs, 2013; Fang et al., 2017; Shahpoury et al., 2021; Yang and Weber, 2022). Fang et al. (2017) showed a series of associations between low aerosol pH, transition metal solubilization, and OP_{DTT} increase due to sulfuric acid.

Zn, for example, is a redox inactive metal with no unpaired electrons in the d orbital and is not involved in a catalytic cycle like Fe and Cu. However, Zn can cause inflammation directly or indirectly because of biological mechanisms in the body (Samet et al., 2020; Wu et al., 2013; Gottipolu et al., 2008); such as the inhibition of the ROS reduction circuit in mitochondria (binding sites for Zn^{2+} on cytochrome C oxidase) (Muramoto et al., 2007; Qin et al., 2007), the inhibition of tyrosine phosphatase (Inflammation inhibition enzyme) activity (Samet et al., 1999), and the induction of inflammatory mediator (IL-8) (Samet et al., 1998). Gottipolu et al., (2008) examined inflammatory markers (increased rate of macrophages and neutrophils) of metals, such as Zn, in tire particles in rat tracheas and found that inflammation did not occur when the water-soluble compartment was low. Furthermore, insoluble components were expelled by mucociliary clearance, whereas soluble metals are bioavailable, leached off in the lung lining, rapidly enter the circulatory system within 24 h, and migrate to extrapulmonary organs

88 such as the heart (Wallenborn et al., 2007). Therefore, the water-soluble fraction of redox-inactive metals
89 is also an important factor in inducing inflammation in biological processes.
90 The road transport and power generation sectors are both major sources of anthropogenic pollutant
91 emissions. However, based on the Paris Agreement, many countries are promoting the spread of
92 renewable energy and next-generation vehicles, such as battery electric vehicles (BEVs), to reduce
93 pollutant emissions. In Japan, the government has set a green growth strategy that aims for carbon
94 neutrality by 2050, targeting the production of 50%–60% of the total electricity demand from renewable
95 energy sources and 30%–40% of it from nuclear power or thermal power using CO2 capture and storage
96 (CCS) technologies. It is also aimed that next-generation vehicles will account for 50%–70% of new
97 passenger car sales by 2030. The renewable energy shift will reduce the emissions of gaseous pollutants
98 and metals derived from fly ash in thermal power plants. The penetration of BEVs will also reduce on-
99 road emissions, and if the electricity is clean (renewable and nuclear electricity), increased upstream
100 emissions will be avoided. However, the case for metals emitted from vehicles is slightly more
101 complicated.
102 The contribution of "non-exhaust" PM emissions, such as brake, tire, and road wear, is becoming
103 more significant as exhaust becomes cleaner (OECD, 2020; Vanherle et al., 2021; CEC, 2022). Brake
104 wear is a major source of metal emissions from automobiles, and metal components (Fe, Cu, Zn, Ba, etc.)
105 account for 35%–47% of the $PM_{2.5}$ particle size wear suspended in the air (Hagino et al., 2016). The most
106 abundant metal in tire treads is Zn, which is added as a vulcanizing agent and accounts for approximately
107 1% of the $PM_{2.5}$ size mass of tire wear particles (Smolders and Degryse, 2002; Blok, 2005; Grigoratos and
108 Martini, 2014). Several reports and review articles have pointed out the risk of non-exhaust PM-derived
109 metals causing the above health effects (Grigoratos and Martini, 2014; Fussell et al, 2022). However,
110 regulations for non-exhaust PM are currently limited to only a few regions (OECD, 2020) and are
111 currently in the process of standardizing emission estimates (EMEP/EEA, 2019) and considering
112 measures.
113 Under this situation, several studies have estimated that BEV proliferation will not bring benefits in
114 terms of non-exhaust PM emissions, which seems to be the consensus (Timmers and Achten, 2016; Alam
115 et al., 2018; OECD, 2020; Beddows and Harrison, 2021; Fussell et al., 2022; Mehlig et al., 2021; Sisani et
116 al., 2022). While the increase in vehicle weight due to the BEV's drive battery increases non-exhaust PM
117 (Timmers and Achten, 2016), the regenerative braking system (RBS) reduces the frequency of friction
118 brake operation and decreases brake wear. Although these changes are depend on additional weight and
119 driving assumptions, an increase due to weight and a decrease due to RBS are estimated to cancel each
120 other out, resulting in a small net change. For example, OECD (2020) estimated that, for lightweight
121 BEVs (range of 100 miles), the benefits of the RBS would dominate the effect of vehicle weight increase,

122 reducing $PM_{2.5}$ by approximately 11%–13%, while heavy BEVs (range of 300 miles) would increase
123 $PM_{2.5}$ by 3%–8% because the significant weight increase would mainly increase tire wear. Beddows and
124 Harrison (2021) reported that the advantages of the RBS do not offset the disadvantages of vehicle weight
125 increase in highway driving, although they are reduced in urban and rural areas where braking occurs
126 more frequently than with internal combustion engine vehicles (ICEVs) (−26% and −12%, respectively).
127 Alam et al. (2018) evaluated fleet-based CO_2 and $PM_{2.5}$ emission trends based on a BEV penetration
128 scenario in Ireland through 2035. They estimated that $PM_{2.5}$ emissions will decrease until about 2028 due
129 to exhaust gas reductions, but then will begin to increase mainly due to the growing due to the increased
130 contribution of non-exhaust PM.
131 However, the relative weight ratios of BEVs to ICEVs in these studies were based on current
132 assumptions. In reality, it is assumed that vehicle lightweighting technologies, including batteries for
133 BEVs, will advance in the future (Moawad et al., 2011; Moawad et al., 2016; Kelly et al., 2015), but no
134 quantitative evaluation of their effects on non-exhaust PM emissions has been conducted. Furthermore,
135 all of the above studies were based on $PM_{2.5}$ emissions, and none of them estimated changes in emissions
136 or atmospheric concentrations of metal components with high oxidative stress risks. Several studies have
137 conducted to evaluate the impacts of next-generation vehicle penetration on atmospheric $PM_{2.5}$
138 concentrations using 3-dimensional numerical modeling, but the primary emissions of non-exhaust PM
139 were not considered (Tessum et al., 2014; Li et al., 2016; Ke et al., 2017) or assumed to be the same as for
140 ICEVs (Soret et al., 2014; Pan et al., 2019; Schnell et al., 2019). Only Nopmongcol et al. (2017) assumed
141 that the brake wear emissions from BEVs and plug-in hybrid electric vehicles (PHEVs) are 25% lower
142 than those from conventional vehicles, but again, the evaluation was based on only the $PM_{2.5}$ mass
143 concentration.
144 In this study, the impacts of changes in primary emissions associated with the renewable energy
145 shift, passenger car electrification, and lightweighting through 2050 on not only the mass concentration of
146 $PM_{2.5}$ in the atmosphere, but also those of metal species (Fe, Cu, and Zn) and aerosol acidity that cause
147 respiratory system oxidative stress and inflammation, were evaluated using chemical transport modeling
148 (CTM). In Section 2, the methodology is explained, including an overview of the CTM, observational
149 data for model evaluation, and assumptions for sensitivity experiments. In Section 3, the reproducibility
150 of the model is verified first. Then, the impacts of renewable energy shifting, passenger car electrification,
151 and lightweighting on the concentrations of the $PM_{2.5}$ total mass, Fe, Cu, and Zn and aerosol pH are
152 evaluated. By integrating these results, changes in water-soluble metal concentrations are discussed. In
153 Section 4, we present conclusions and discuss future work.
154

2. Materials and Methods

2.1. Regional meteorology–chemistry model

A regional-scale offline-coupled nonhydrostatic meteorology–chemistry model (NHM-Chem) (full chemistry version; Kajino et al., 2019a; 2021 and transition metal version; Kajino et al., 2020) was used in this study. Detail descriptions are summarized in Table S1. Figure 1 shows the model calculation domains. The mother domain (domain 01) covered the Northeast Asian region and was calculated with dx = 30 km. The nested domain (domain 02) covered Japan from Kyushu to Tohoku regions with dx = 6 km. The vertical layer involved 40 layers up to an altitude of approximately 20 km in both domains. Hereafter, the model simulation results were of the lowest level (approximately 15 m above the ground level) unless otherwise noted. The calculation period was from January 1, 2015, to December 31, 2015; the simulation began on December 26, 2014, with a spin-up period of 5 days.

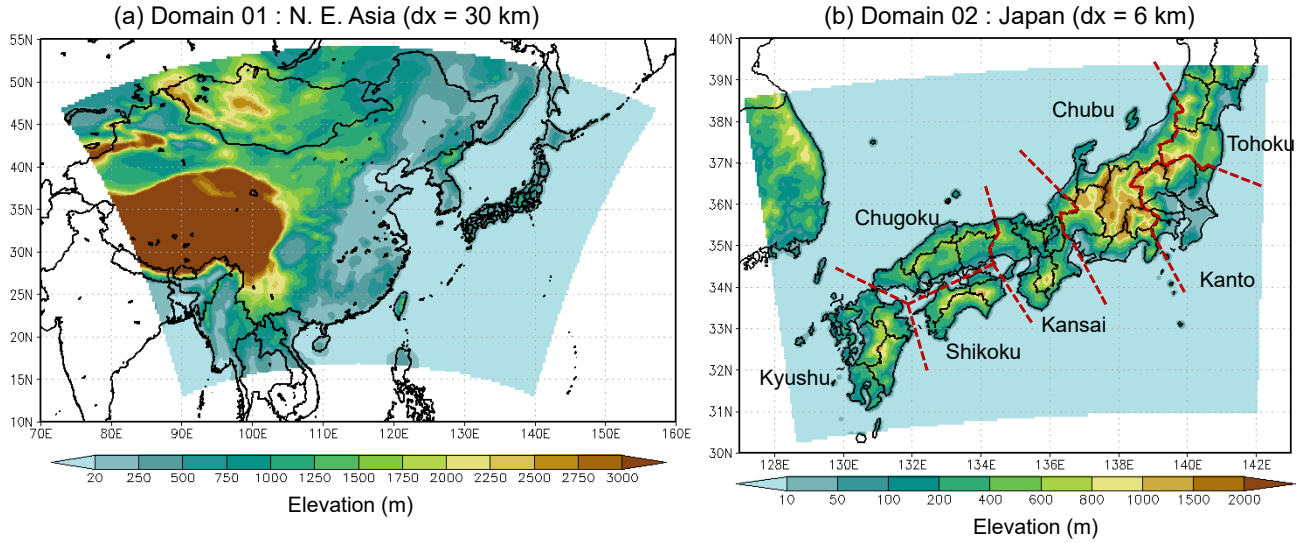

Figure 1. Model domains in this study. (a) Terrestrial elevations of domain 01 (Northeast Asia, dx = 30 km) and (b) same as (a) but for domain 02 (Japan, dx = 6 km).

First, the emission inventories used for gas and particle calculations for the full chemistry version model are described. For Northeast Asian anthropogenic emissions, REAS v3.2.1 (minor change in December 2021 from v3.2 (Kurokawa and Ohara, 2020), 0.25° × 0.25°, base year = 2015) and for Japan, PM2.5EI (Morikawa, 2017, 1 km × 1 km, base year = 2012) were used. NO_x emissions were allocated 9:1 to NO and NO_2 for both REAS v3.2.1 and PM2.5EI. Taking chimney elevation into account, emissions from industries and power plants were distributed in this study from 0 m to 300 m above the ground level. We assumed the following for the original DB of PM2.5 EI in this study.

- In the PM2.5EI, since there is no information on the mass fraction of "brake wear" in "road dust (including brake wear)", it was assumed to be 0.35 based on the value calculated by EMEP/EEA

(2019). The EMEP/EEA air pollutant emissions inventory guidebook (2019) was published by the European Environment Agency (EEA) and supports the reporting of emissions data under the UNECE convention on long-range transboundary air pollution (CLRTAP) and the EU national emissions control directives. In this study, the remainder of "road dust (including brake wear)" minus "brake wear" is called "road wear and resuspension".

- In the PM2.5EI, non-exhaust PM emissions from automobiles are not classified by particle size (those from other sources are classified as $PM_{2.5}$ or PM_{10}). In this study, the $PM_{2.5}$/PM_{10} mass fraction of non-exhaust PM was assumed to be 0.35 based on hearing information from JCAP/JATOP and the estimated data of EMEP/EEA (2019). EMEP/EEA (2019) estimated the $PM_{2.5}$ fraction for tire wear, brake wear and road surface wear to be 0.42, 0.39 and 0.27, respectively, their mean is approximately 0.35. NHM-Chem assumes a log-normal distribution for the PM particle size distribution at emission. By setting the parameter of number-equivalent geometric mean dry diameter = 0.80 μm (number-equivalent aerodynamic mean dry diameter = 1.13 μm), and standard deviation = 1.8, the aerodynamic $PM_{2.5}$ fraction is approximately 0.35.
- Since our available PM2.5EI data do not provide information on the mass fractions of BC and OC in $PM_{2.5}$ and PM_{10} emissions, we applied the corresponding REAS v3.2.1 mass fractions for each sector of PM2.5EI. The remaining primary PM emissions, excluding BC and OC, were defined as inert unidentified components (UIDs).
- For domain 2 over Japan, the ship emissions from EAGrid (Fukui et al., 2014; Kannari et al., 2007) were added because PM2.5EI does not provide ship emissions.

GFED v4 (Giglio et al., 2013) was used for biomass burning emissions and JMA data was used for volcanic SO_2 emissions for both domains. Biogenic nonmethane volatile organic compound (NMVOC) emissions were calculated inline based on MEGAN v2 (Guenther et al., 2006) as a function of temperature and solar radiation, simulated by the meteorological model.

The transition metal version of the model simulated 10 metals (Cu, Mn, Co, V, Ni, Pb, Fe, Zn, Cd, and Cr) in three categories (anthropogenic $PM_{2.5}$ metals, anthropogenic PM_{10} metals, and Asian mineral dust metals). The anthropogenic emission inventory used for the simulations of $PM_{2.5}$ and PM_{10} metals was TMI-Asia/Japan v1.1, developed in this study. The previous version (v1.0; Kajino et al., 2020) contained considerable discrepancies between simulated and observed metal concentrations, especially for Cu and Zn, which were substantially improved in this revision. In addition, TMI-Asia v1.0 did not consider metals from all non-exhaust PM (brake wear, tire wear, road wear and resuspension), but they were added in v1.1 (note that only Fe, Cu, and Zn were considered for road wear and resuspension). TMI-Japan v1.0 considered brake and tire metal emissions but did not consider those from road wear and resuspension, which were added in v1.1. The details of the revisions from v1.0 to v1.1 are described in

Supporting Text S1, Figure S1–S4, and Table S1–S3. TMI-Asia/Japan were developed by multiplying sector-specific $PM_{2.5}$ or PM_{10} emission estimates from REAS v2 (Kurokawa et al., 2013, 0.25° × 0.25°, base year = 2008) and PM2.5EI by metal content, respectively. However, in TMI-Japan, brake, tire, and railway-derived metals were based on PM emission estimates from EAGrid (1 km × 1 km, base year = 2010). The metal content of PM by sector is an average of several literature values registered in SPECIATE v4.4 provided by the USEPA. The list of metal content by sector used in TMI-Asia/Japan v1.1 is shown in the Supporting excel data. The metals in Asian mineral dust particles were diagnosed from the simulated dust mass concentration and the metal profiles of the Certified Reference Material of the National Institute for Environmental Studies (NIES CRM No. 30; Gobi Kosa) (Nishikawa et al., 2013).

For the initial and boundary conditions for the NHM (meteorological model part of NHM-Chem), we used a 6-hourly JRA-55 global reanalysis dataset (Kobayashi et al., 2015) for domain 01 and 3-hourly JMA's Meso-Regional Objective Analysis (MA) for domain 02 (available at https://www.jma.go.jp/jma/jma-eng/jma-center/nwp/nwp-top.htm, last accessed: 20 January 2023). For the large-wave components of horizontal momentum and potential temperature (wavelengths >1,000 km), spectral nudges above a 7-km altitude were applied, and the weighting factor was set to 0.06. For the chemical transport model (CTM) part of NHM-Chem, monthly climatological values (10-year averages for the global models MRI-CCM2 and MASINGAR-mk2 from 2003 to 2013) were used for the initial and boundary concentrations in domain 01, and the results of domain 01 were used for domain 02. The input/output time interval of CTM was 1 h.

2.2. Aerosol pH calculation

The aerosol pH discussed in Section 3.2.2 was derived using ISORROPIA-II (Fountoukis and Nenes, 2007). ISORROPIA-II can simulate the thermodynamic equilibrium of water-soluble inorganic ions and calculate the pH of aerosol particles in the equilibrium state. ISORROPIA-II was implemented in NHM-Chem for the calculation of the condensation of HNO_3, NH_3, HCl, and H_2O (Kajino et al., 2021), but aerosol pH was not dynamically solved. In addition, ISORROPIA-II in NHM-Chem solves the aerosol thermodynamics of each aerosol category but does not solve the aerosol pH of bulk submicron aerosols discussed in the study. Thus, a standalone ISORROPIA-II model was used to diagnose the aerosol pH after the NHM-Chem simulation. In addition, sensitivity tests of Equations (5)–(7) were only feasible using this standalone model.

The $PM_{2.5}$ particle size aerosol pH was derived as follows. First, the forward mode of ISORROPIA-II was run using hourly NHM-Chem calculation results as input data; the mass concentrations (mol m^{-3}) of K^+, Ca^{2+}, Mg^{2+}, NH^{4+}, Na^+, SO_4^{2-}, NO_3^-, and Cl^- in the submicron category (aitken, soot-free

accumulation, and soot containing accumulation modes), relative humidity (RH), and temperature. The output of the 1-hour aerosol liquid water content (LWC) and hydronium ion concentration data for each model grid were monthly averaged and applied to the following equation (1) for defining monthly averaged aerosol pH:

$$pH = -\log_{10}\left(\gamma_{H^+} \cdot H^+_{aq}\right) = -\log_{10}\left(\frac{1000\gamma_{H^+} \cdot H^+_{air}}{LWC}\right) \quad (1)$$

where γ_{H^+} is the activity coefficient of hydronium ions (assumed =1), H^+_{aq} is the concentration of hydronium ions in the aerosol water phase (mol L^{-1}), H^+_{air} (μg m^{-3}) is the concentration of hydronium ions per air volume, and LWC (μg m^{-3}) is the water concentration of aerosol particles. However, only 1-h data corresponding to 20% < RH < 95% were used for the monthly average. Data with RH < 20% were excluded because the aerosol was unlikely to be in a liquid state and the activity coefficient of hydronium ions in the aerosol water phase was highly uncertain at the case of high concentrations under low RH conditions (Fountoukis et al., 2009; Guo et al., 2016). The LWC increases exponentially with increasing RH due to the hygroscopicity of NH_4NO_3 and $(NH_4)_2SO_4$ (Kitamori et al., 2009). Data with RH >95% were excluded because the uncertainty in RH could significantly increase the uncertainty in LWC and aerosol pH (Guo et al., 2015; Guo et al., 2016). The LWC mainly depends on hygroscopic inorganic species, such as sulfate. Organics have relatively low hygroscopicity, so their effect on aerosol pH is small and can be neglected (Guo et al., 2015; Vasilakos et al., 2018 ; Pye et al., 2018). Similar to many other studies (Lawal et al., 2018; Ding et al., 2019; Paglione et al., 2021), this study did not consider the impact of organic matter on aerosol pH. Instead, the uncertainty in aerosol pH due to unaccounted for organic matter is described in Supporting Text S2 and Figure S5.

2.3. Model experiment cases and parameter setting

2.3.1. Model experiment cases

A base experiment and the following three sensitivity experiments were conducted in this study. The emissions for each sensitivity experiment were determined by scaling the base experiment by the coefficients shown in Table 1. Our previous study (Kayaba and Kajino, 2022), which estimated the impact of the BEV shift of all passenger vehicles on surface O_3 concentration, did not consider scenarios of changes in vehicle type mix or power supply mix over time. However, we developed detailed future scenarios based on the aims of the Japanese government in this study. The coefficients were derived based on the estimated trends in vehicle exhaust and non-exhaust emissions, and gasoline and electricity demands through 2050. The details of the process of derivation are described in Sections 2.3.2–2.3.4.

(1) BASE experiment.

278 The simulation period was the whole year 2015, and the emission amounts of the base year (2010–
279 2015) values were used for the simulation (Table S1).
280 (2) 2050R experiment; assumption of the penetration of renewable energy through 2050.
281 This scenario assumed the penetration of renewable energy, taking into account changes in the power
282 supply mix through 2050. The emissions from power plants were reduced considering the decrease in
283 thermal power generation.
284 (3) 2050R&E experiment; assumption of the penetration of renewable energy and passenger car
285 electrification through 2050.
286 This scenario assumed passenger car electrification (without lightweighting) through 2050 in addition
287 to (2). Changes in exhaust/non-exhaust emissions due to changes in vehicle type mix (ICEV, hybrid
288 electric vehicle (HEV), PHEV, and BEV) were considered. To assess the impact of passenger car
289 electrification, the assumptions for heavy-duty vehicles were not changed. Also, the total number of
290 vehicles owned and the volume of traffic were not changed to evaluate the sensitivity of changes in
291 emission factors. The additional electricity demand for charging BEVs and PHEVs was estimated to
292 be mostly covered by solar surpluses, although not completely, resulting in a slight increase in power
293 plant emissions of 1% from (2). NMVOC emissions from gas stations were reduced due to the
294 reduced demand for gasoline.
295 (4) 2050R&E&L experiment ; assumption of the penetration of renewable energy and passenger car
296 electrification and light-weighting through 2050.
297 This scenario considered passenger car lightweighting through 2050 in addition to (3). Non-exhaust
298 emissions were reduced from (3) due to vehicle weight reduction. It was assumed that exhaust
299 performance would not change due to lightweighting. No increase in power plant emissions was
300 assumed (same as (2)), because the additional electricity demand for charging BEVs and PHEVs was
301 estimated to be lower than that in (2) because of the lower electricity consumption due to
302 lightweighting, which can be covered by the surplus of solar power. NMVOC emissions from gas
303 stations were further reduced compared to that in (3) due to the improved of energy consumption by
304 vehicle lightweighting.

305

Table 1. Ratios of emission factors for the sensitivity experiments (2050R, 2050R&E, and 2050R&E&L) to BASE experiment.

Emission source	species		BASE	2050R	2050R&E	2050R&E&L
	particle pollutants	gaseous pollutants				
Passenger car exhaust	$PM_{2.5}$, Fe, Cu, Zn	SO_x, NO_x, NH_3, NMVOC[a], CO	1	1	0.31[b]	0.31[b]
Passenger car evaporative	-	NMVOC[a]	1	1	0.31[b]	0.31[b]
Passenger car tire wear	$PM_{2.5}$, Zn	-	1	1	1.09[c]	0.89[c]
Passenger car road wear & resuspension	$PM_{2.5}$, Fe, Cu, Zn	-	1	1	1.09[c]	0.89[c]
Passenger car Brake wear	$PM_{2.5}$, Fe, Cu, Zn	-	1	1	0.67[d]	0.55[d]
Thermal power plant	$PM_{2.5}$, Fe, Cu, Zn	SO_x, NO_x, NH_3, NMVOC[a], CO	1	0.18[e]	0.19[e]	0.18[e]
Gas station	-	NMVOC[a]	1	1	0.41[f]	0.33[f]

a. SOA formation was not included in the simulations. Therefore, changes in NMVOC emissions only affected changes in oxidant concentrations such as O_3, OH, and H_2O_2, and the associated changes in secondary inorganic aerosol formation.
b. Passenger car electrification was considered (Figure 4d)
c. Passenger car electrification and lightweighting were considered (Figure 4b)
d. Passenger car electrification, lightweighting, and effect of BEV's RBS were considered (Figure 4c)
e. The reduction of thermal power plants was considered (see Figure S1b). No increase in thermal power plant emissions was assumed because it was assumed that the additional electricity demand for charging BEVs and PHEVs (Figure 4e) could be covered by the surplus electricity obtained solar power generation.
f. The reduction of gasoline consumption was assumed (Figure 4f).

Table 2 shows the assumptions that were changed and unchanged from the BESE experiment.

Table 2. Assumptions that were changed or unchanged in the 2050R&E&L experiment compared to the BASE experiment.

Sector	Changed	Unchanged
Vehicle transport	✓ Vehicle type mix (passenger car) ✓ Vehicle lightweighting (passenger car) ✓ Energy consumption (passenger car)	✓ Assumption of truck, bus and motorcycle ✓ Total traffic volume ✓ Total vehicle stock
Power plant	✓ Power supply mix ✓ Additional electricity demand for BEV and PHEV charging	✓ Electricity demand excluding BEV and PHEV charging
Stationary VOC	✓ Gasoline fuel demand at gas stations	✓ Assumption of other stationary VOC source
Other sectors[a]	-	✓ All assumptions

a. Industry, domestic, aviation, navigation, railway, off-road vehicle, and field-burning

2.3.2. Passenger car lightweighting through 2050

Figure 2 shows the change in vehicle weight for each vehicle type through 2050. For each of the four vehicle types (ICEV, HEV, PHEV, and BEV), the weights of six components (body frame, tire, engine, transmission, motor/generator, fuel tank, and drive battery) are combined. Each component weight was referenced to calculations conducted by Autonomie, a vehicle simulation tool developed by the Argonne National Laboratory (ANL) of the U.S. Department of Energy (Moawad et al., 2016; Islam et al., 2020). Autonomie can evaluate vehicle weight, fuel consumption, performance, and cost for various vehicle classes (mini, medium, small sport utility vehicles (SUV), medium SUV, and pickup truck) and vehicle types (ICEV, HEV, PHEV, BEV, and fuel-cell electric vehicle (FCV)). In this study, only the body frame and the drive battery were assumed to be lightweight through 2050 (their reduction rates are shown in Table S4 and Table S5, respectively). The lightweighting of body frames can be achieved by alternative materials, such as high-strength low-alloy steels and aluminum and will be relatively early in the future. Compared to 2020, approximately –10% will be achieved by 2025, followed by a gradual decrease, with a lightweighting of approximately 20% in 2050 (Table S4). As the energy density of the battery increases, the weight per unit capacity decreases for the fixed driving range. Approximately 43% lighter body frames were expected in 2050 than in 2020 (Table S5). The battery weight of the PHEV was assumed to be 1/3 of that of the BEV in this study. The weights of other components such as the engine and motor/generator were assumed to be unchanged. Until 2020, BEVs were net 14% heavier than ICEVs due to their batteries. By 2050, ICEVs and HEVs will be 15% lighter compared to those in 2020 due to the lightweighting of the body frame. PHEVs and BEVs have a larger lightweight ratio than ICEVs and HEVs because of the reduction in battery weight in addition to the reduction in body frame. After 2030, BEVs and PHEVs will be lighter than ICEVs produced in 2015. By 2050, the weight difference between vehicle types will be smaller, with a +5% relative weight difference for BEVs compared to ICEVs.

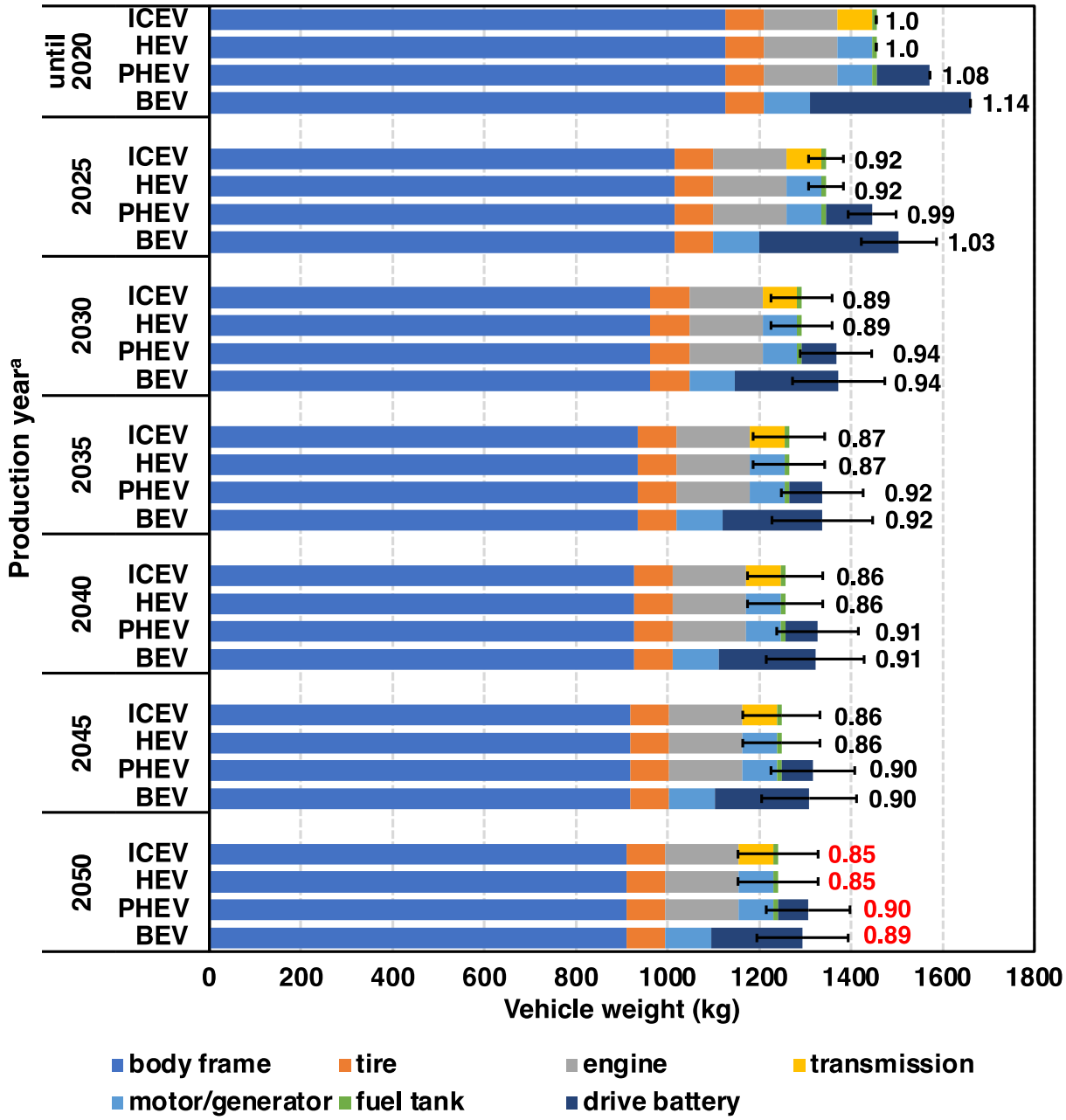

Figure 2. Vehicle weight transition of each vehicle type through 2050 due to lightweighting. The numbers shown along with the bars represent the values relative to ICEVs produced until 2020. The error bars indicate the uncertainty in the degree of the technological progress of lightweighting (low and high). The weight of each component in the base year (until 2020) was based on literature values derived using Autonomie (Moawad et al., 2016). Only the glider and the drive battery were assumed to be lightweight (weight reduction rates are shown in Tables S4 and Table S5, respectively), while the weights of other components remained unchanged.

2.3.3. Vehicle type mix through 2050

It is necessary to estimate fractions of each vehicle type and its production year at the same time in the passenger car fleet in 2050 since the year of vehicle production affects fuel economy and vehicle weight. In this study, the vehicle turnover was estimated as a function of scrapping rate according to vehicle age, and the trend in the vehicle ownership share was predicted, as shown in Figure 3a. Figure S6 shows the vehicle type mix of new passenger car sales through 2050. This was estimated based on Sato and Nakata (2020) (based on data published by the METI, JAMA, and the Next-Generation Vehicle Promotion Center (NGVP)). Although FCVs are expected to account for approximately 5% of the total sale share in 2050, FCVs were excluded from this study since they are not majors. Figure S7 shows the scrap and residual rates as a function of vehicle age, derived by the Weibull functions shown in Equations (2) and (3). The Weibull function was first proposed by Weibull (1951), and it statistically represents the phenomenon of machine deterioration. It is widely used in the field of reliability engineering and has been used for modeling vehicle survivability (Hao et al., 2011).

$$R(t) = \exp\left(-\left(\frac{t}{\eta}\right)^{m}\right), \quad (2)$$

$$f(t) = \frac{m \cdot t^{m-1}}{\eta^{m}} \cdot exp\left\{-\left(\frac{t}{\eta}\right)^{m}\right\}, \quad (3)$$

where $R(t)$ is the survival ratio at age t (years), and $f(t)$ is the scrap ratio at age t (years). η is called scaling parameter and is defined as the average vehicle lifetime. Assuming $t = \eta$ and substituting it into Equation (2), we obtain the residual $R(t) = 1/e$. m is called Weibull coefficient. In this study, $\eta = 12.7$ and $m = 4.0$ were used to reflect the residual pattern of ordinary vehicles in Japan (Lu et al., 2018). These values were derived by Lu et al (2018) through regression against the patterns of residual rates derived from data on the numbers of registered and scrapped ordinary vehicles in Japan reported by Huo and Wang (2012). Figure 3a shows the vehicle type mix by production year for the total passenger car fleet in Japan through 2050. It was derived by assuming that cars are replenished by the share of new car sales in that year (Figure S6) for the number of scrapped cars in each year derived in Equation (2). The estimated vehicle ownership share in 2050 was 11% for ICEVs, 14% for HEVs, 20% for PHEVs, and 55% for BEVs (Figure 3a).

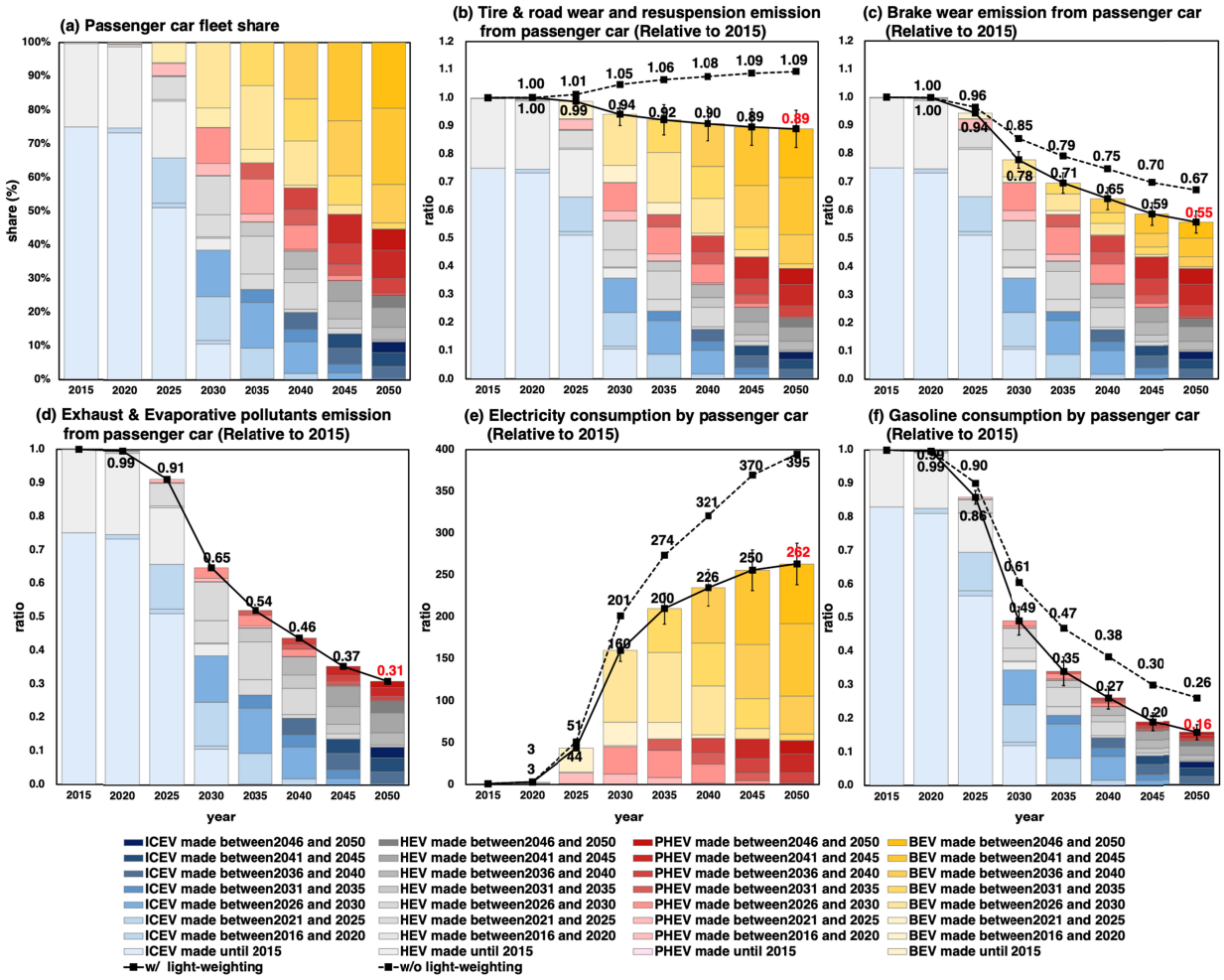

Figure 3. Trend in (a) passenger car fleet share, (b) tire and road wear and resuspension emission, (d) brake wear emission, (e) gasoline fuel consumption, and (f) electricity consumption through 2050. Each graph shows values relative to 2015. The bar graph and the solid black line indicate the transition with vehicle lightweighting, and breakdown by production year and vehicle type is shown. The dashed black lines indicate the transition without vehicle lightweighting. The error bars indicate the uncertainty due to the degree of the technological progress of lightweighting (Figure 2). Since it is assumed that exhaust gas pollutants do not change with lightweighting (see Section 2.3.4.2), the error bars are not indicated in (d).

392 ### 2.3.4. Change in emissions through 2050
393 #### 2.3.4.1. Non-exhaust PM emissions from passenger car

394 The emissions of "tire and road wear and resuspension" and "brake wear" in the 2050R&E&L
395 experiment were estimated to be 89% and 55% of those in the BASE experiment, respectively (Figure 3b
396 and 3c solid line). Figure 3b and 3c were derived by weighting the vehicle type mix by production year in
397 Figure 3a by the vehicle weight in Figure 2 since both non-exhaust PM emissions are proportional to
398 vehicle weight (Simons, 2016). The brake wear was then further multiplied by 0.33 to take into account
399 the effect of regenerative braking for BEVs only. In the friction brake system (FBS) used in conventional
400 vehicles, excess kinetic energy during braking is discarded as heat. In contrast, the RBS in BEVs can
401 recover braking force by converting it into electrical energy. In BEVs, the combined use of the FBS and
402 the RBS can reduce brake disc wear. Various values have been reported in the literature regarding the
403 effectiveness of the RBS in reducing brake wear (Table 3). The value indicated by Hagino (2019), −67%,
404 was adopted of these literature values in this study. This is because PM emissions are directly measured
405 by the Particle Measurement Program (PMP) test cycle, an expert working group for brake wear
406 measurement, and non-asbestos organic (NAO) brake pad material, which is the most common material
407 used in Japan (accounts for approximately 70% share of passenger cars), is used. The brake wear
408 reduction effect of the RBS was assumed to be −67%, even if the vehicle weight changed.

409 Primary emissions from tire and road wear and resuspension will be reduced to approximately 10%
410 by around 2035 because of the body frame lightweighting of ICEVs and HEVs, but the reduction will
411 stall after that (Figure 3b solid line) because BEVs will not be relatively lighter than ICEVs, HEVs, and
412 PHEVs even in the future. As mentioned in Section 2.3.2, BEVs have a large rate of lightweighting and
413 will be lighter than ICEVs produced in 2015 by 2030, so it was estimated that tire and road dust
414 emissions will not increase in the future from the 2015 level.

415 In the case of the 2050R&E experiment, PHEVs are 8% heavier and BEVs are 14% heavier than
416 ICEVs without considering future weight reductions (Figure 2). Therefore, the increase in the share of
417 PHEVs and BEVs is estimated to increase tire and road wear and resuspension by 9% in 2050 relative to
418 the reference experiment (Figure 3b dashed line). This is a disadvantage of BEVs, as mentioned in the
419 Introduction. However, our estimation suggests that the disadvantages can be suppressed by
420 lightweighting the body frame and battery (Figure 3b solid line).

421 Brake wear emissions will be reduced by 33% in 2050 compared to that in 2015 due to the
422 penetration of BEVs even without considering vehicle lightweighting (Figure 3c dashed line) but can be
423 reduced by 44% with lightweighting (Figure 3c solid line).

424

Table 3. Literature values for brake dust reduction owing to the regenerative braking of BEVs. Much of this information is summarized in OECD (2020).

Sector	Reported reduction ratio	Unchanged
Barlow, 2014	almost −100%	Visual confirmation (Brake components look new after 22,000 miles)
Hooftman et al., 2016	–40%	Replacement interval of brake pads (BEV's brake pad last approximately two-thirds longer than that of diesel/petrol vehicles, in case of Tesla BMW i3 and LEAF)
Platform for Electro-mobility, 2016	–25 – –50%	Information provided by company (Brake pad reduction ratio in case of Renault ZOE)
Kendrick and Kulkarni, 2019	–50%	Laboratory test (WLTP[a] driving cycle and semi-metallic brake pad)
Hagino., 2019	–67%	Laboratory test (PMP[b] driving cycle and NAO[c] brake pad)
Hall, 2017	–88%	Los Angeles city traffic test (LACTT)[d] (The frequency of friction braking for BEVs was 1/8 of that for ICEVs of the same vehicle class.)

a. Worldwide-harmonized light vehicles test procedure
b. Particulate measurement program
c. Non-asbestos organic
d. LACTT is an established procedure used almost universally for generations by vehicle manufacturers to evaluate and validate braking systems (Hall, 2017).

2.3.4.2. Exhaust gas and PM emissions from passenger car

The emissions of gaseous pollutants such as NO_x from passenger car exhaust will decrease as the fractions of BEVs and PHEVs increase. The emissions of exhaust gas pollutants in the 2050R&E and 2050R&E&L experiments were assumed to be 31% of those in the BASE experiment (Figure 3d). It was assumed that the emission factors of exhaust pollutants would not change even if fuel consumption was improved due to lightweighting. In addition, the emission factors for exhaust pollutants from gasoline driven HEVs and PHEVs were assumed to be the same as those for ICEVs. This is because while improved fuel consumption reduces CO_2 emissions, but this is not true to trace pollutants such as NO_x. HEVs are often driven by a motor using electricity generated by running the engine at low load and low speed. The low power operation of the engine may reduce exhaust emissions, but it may also increase emissions as the aftertreatment system takes longer to warm up and the catalyst stays at a lower temperature (Zhao and Wang, 2016).

For PHEVs, the ratio of electric driving to gasoline driving was assumed to be 7/3. The PHEV runs by externally charged electric power for a certain distance from the start of driving with a small drive battery of approximately 10 kWh and switches to engine-driven hybrid running when the battery's state of charge (SOC) decreases to a certain value. The ratio of electric drive to the total daily driving distance is called the utility factor (UF) (Society of Automotive Engineers J2841 standard). Since the UF varies by person and by day, previous studies have derived the average UF of PHEVs in Japan based on the

451 statistical data of the daily distance traveled by PHEV users. It is estimated that the UF = 0.7 when
452 assuming a PHEV with an electric driving range of 60 km, as represented by the Prius PHV (Hori and
453 Kaneda, 2012). Therefore, the electric driving ratio of PHEVs was assumed to be 70% in this study as
454 well.
455
456 **2.3.4.3. Upper-stream emissions (thermal power plant and gas station)**

457 The Japanese government expects an increase in renewable energy and a decrease in thermal power
458 generation in the future in order to decarbonization. The emissions from power plants in the 2050
459 R&E&L experiment were assumed to be 18% of those obtained from the BASE experiment.

460 • The power supply mix in 2050 was estimated to be 50% renewable energy, 34% nuclear, and
461 16% thermal, provided that the government targets would be achieved (Figure S8b).
462 • Thermal power generation, which provided 89% of the total electricity demand in 2012 (the
463 PM2.5 EI base year) (Figure S8a) (METI, 2019) would decrease by 82% by 2050.

464 The change in air pollutant emissions due to the introduction of CCUS in thermal power plants
465 strongly depends on the type of CO_2 capture technology employed (EEA, 2011) (Supporting Text S4).
466 Furthermore, there are many uncertainties, including future innovations in denitrification and
467 desulfurization technologies and regulatory changes, so estimating the changes in emission factors of
468 thermal power plants is difficult. Therefore, the emission factors for pollutants from thermal power plants
469 were assumed to remain the same in 2050 as in the base year.

470 No increase in power plant emissions was assumed for charging BEVs and PHEVs since it will be
471 met by solar surplus electricity in 2050 (Supporting Text S5). Figure 3e shows the electricity demand for
472 external charging for passenger cars considering the improvement of fuel and electricity consumption
473 (Table S6) due to electrification and lightweighting in 2050. The external charging electricity demand
474 was negligible in 2015, as the share of BEVs and PHEVs in the total passenger car fleet was very small,
475 approximately 0.2% (NGVP's website: https://www.cev-pc.or.jp/tokei/hanbaidaisu.html; Automobile
476 Inspection & Registration Information Association (AIRIA)'s website:
477 https://www.airia.or.jp/publish/statistics/trend.html, both in Japanese, last accessed: 22 January 2023).
478 The additional electricity demand was only 0.02% of the total annual domestic electricity generation
479 (107.78 billion kWh $year^{-1}$; METI, 2019), assuming a total annual passenger car fleet of 420 billion
480 km/year (MLIT, 2010) and an electricity consumption of 0.17 kWh km^{-1} for BEVs and PHEVs. In 2050,
481 the demand for externally charged electricity will increase by 260 times (Figure 3e solid line) due to the
482 penetration of BEVs and PHEVs, which increase the total electricity demand by 4% in Japan. However, it
483 was estimated that this additional electricity demand could be met by surplus PV power (even in winter
484 when solar radiation is low) (Figure S8b). Without considering the improvement of electricity

485 consumption due to lightweighting (2050R&E experiment), more electricity would be required for
486 charging (395 times more than that in 2012 (Figure 3e dashed line), and 6% increase in the total demand).
487 This may not be covered by some surplus power in the winter, but the increase in thermal generation
488 would be approximately 1% at worst (Supporting Text S5).
489 The electrification and lightweighting of passenger cars will also reduce gasoline consumption. The
490 decreasing refueling frequency will reduce fuel evaporation VOCs at gas stations. Figure 3f shows the
491 gasoline demand by passenger cars. Gasoline consumption by passenger cars accounts for 80% of the
492 total gasoline consumption (MLIT, 2012). With (without) vehicle lightweighting, it was estimated that
493 electrification would reduce gasoline consumption in passenger cars by 84% (74%) (Figure 3f, solid
494 (dashed) line) and VOC evaporation from gas stations by 0.33 (0.41) times compared to those in the
495 BASE experiment.
496

497 ### 2.4. Observation data for model validation

498 To validate the simulation results, nationwide seasonal observation data of Ministry of Environment
499 (MOE), Japan, were used (available at http://www.env.go.jp/air/osen/pm/monitoring.html, last accessed:
500 January 25, 2023)). The survey was conducted at 192 stations in Japan in 2015 (158 public, 44 roadside,
501 and 15 background sites). During a period of 2 weeks × 4 seasons for a total of 56 days, daily
502 concentrations of 32 inorganic elemental components (Cu, Fe, Mn, Ni, Pb, V, Zn, etc.), and 9 ionic
503 components (NO_3^-, SO_4^{2-}, NH_4^+, Na^+, K^+, Mg^{2+}, Cl^-, Ca^{2+}, and $C_2O_4^{2-}$) were analyzed. The
504 meteorological fields (temperature, pressure, wind speed, and solar radiation) were also measured. The
505 inorganic elemental components other than Si were mainly measured using inductively coupled plasma-
506 mass spectrometry (ICP-MS) after acid decomposition with nitric acid, hydrofluoric acid, hydrogen
507 peroxide, etc. The ionic components were analyzed using ion chromatography. In this study, simulated
508 values from four model grids adjacent to the observation point were weighted inversely proportional to
509 the square of distances and used for comparison with the observations.
510
511

3. Result and Discussion

3.1. Model evaluation

First, the reproducibility of metal concentrations is discussed. The scatter plots and comparative statistics of the simulation results and observations for Fe, Cu, and Zn in $PM_{2.5}$ are shown in Figure S1 and Table S2, respectively. The biases for Cu and Zn were significantly improved by the revision of the transition metal emission inventory TMI-Asia/Japan from v1.0 to v1.1 in this study (Figure S1, Table S2). In v1.0, the NMB of Cu ranged from 130% (roadside site) to 680% (background site) but improved to approximately 30% after the revision. In addition, the NMB at the Zn at the background site improved from approximately 100% to –5% (Table S2). Therefore, the metal bias is within approximately 30% for Fe, Cu, and Zn (refer to Supporting Text S1 for details). The correlation coefficients are R = 0.37, 0.20, and 0.25 for Fe, Cu, and Zn, respectively, and these were relatively high at the background site, R = 0.51, 0.35, and 0.50, respectively (Table S2), indicating that the model well reproduces the temporal concentration variations caused by advection from the continent. On the other hand, values were lower at the roadside sites, R = 0.28, 0.14, and 0.30. One possible cause is the dissociation between inventory and daily actual emissions. Therefore, this study is discussed on a monthly or annual average concentration basis.

Next, $PM_{2.5}$ concentrations and their ionic components in full chemistry simulations are described. The scatter plots and comparative statistics of the simulated and observed $PM_{2.5}$ total mass concentrations and ionic components (SO_4^{2-}, NO_3^-, NH_4^+, Cl^-, Na^+, Ca^{2+}, and Mg^{2+}) are shown in Figure S9 and Table S7, respectively. The model overestimated $PM_{2.5}$ mass concentrations by approximately 60% throughout the year (Table S7). As for the main ionic components, the NMBs of SO_4^{2-} and NH_4^+ are –13% and –9%, respectively, but NO_3^- is overestimated at 247% (Table S7). The overestimation of NO_3^- is significant in summer (NMB = 94%, 199%, 2008%, and 234% in winter, spring, summer, and fall, respectively) (Table S7, Figure S9c). The counter ions of NO_3^- are considered to be predominantly Na^+ derived from sea salt particles. NHM-Chem defines Cl^-, Na^+, and Mg^{2+} concentrations as the ratios of sea salt particle concentrations and Na^+, Mg^{2+}, and Ca^{2+} as the ratios of Asian mineral dust particle concentrations, and these ionic components are not simulated separately. The bias for Ca^{2+} only from mineral dust was within a factor of 2, but the sea salt particle components, Na^+, Cl^-, and Mg^{2+}, were overestimated by a factor of 10 or more (Table S7, Figure S9e–S9h). Therefore, the main cause of the $PM_{2.5}$ overestimation is thought to be the excess of NaCl, mainly due to the uncertainty in the model's sea salt particle generation rate, and the associated excess production of $NaNO_3$ due to chlorine loss ($NaCl + HNO_3 \rightarrow NaNO_3 + HCl$). Other factors such as uncertainties in anthropogenic NO_x and NH_3 emissions and HNO_3 dry deposition rates are also possible.

The model also slightly underestimated the temperature (NMB = −10%) (Figure S10a) and overestimated the RH (NMB = 16%) (Figure S10b). The uncertainties in NO_3^- and RH affect the sensitivity of aerosol pH and thus metal solubility. In this study, when calculating aerosol pH in ISORROPIA-II, the range of uncertainty in aerosol acidity was considered by also inputting the case corrected for bias from observations for the NO_3^- concentration and RH, respectively. And the range of metal solubility due to NO_3^- and RH uncertainties is described in Section 2.3.4.

3.2. Impacts of renewable energy shifting, passenger car electrification, and lightweighting

3.2.1. Impact on primary emissions

3.2.1.1. $PM_{2.5}$ and $PM_{2.5}$-metals

First, the metal content assumptions in $PM_{2.5}$ in TMI-Asia/Japan v1.1 are explained for estimating the primary emissions of metals. Power plants, automobile exhaust, brake and tire wear, and resuspension are shown in Table 4 (for other sectors, see supporting information of Kajino et al., 2020).

The PM of fly ash from coal-fired power plants contains 1.0%–10% Fe, 0.01%–0.1% Cu, and 0.01–0.1% Zn approximately, respectively, in both $PM_{2.5}$ and PM_{10} particle sizes (Chow et al., 2004). In this study, the assumptions for the Fe, Cu, and Zn content in thermal power plant exhaust $PM_{2.5}$ were 4.2%, 0.07%, and 0.3%, respectively.

The gasoline and diesel exhaust gases contain approximately 0.1%–1.0% Fe and Zn and 0.01%–0.1% Cu (Chow et al., 2004). Zn is included because zinc dithiophosphate is added to lubricants as an antiwear and antioxidant (Lough et al., 2005; Cadle et al., 1997). Fe and Cu are included mainly due to bearing wear and other component wear mixing (Cadle et al., 1997). The assumptions for the Fe, Cu, and Zn contents in vehicle exhaust $PM_{2.5}$ in this study were 0.5%–0.7%, 0.03%–0.06%, and 0.2%–0.4%, respectively.

The metal content in brake wear varies widely depending on the brake pad material. NAO, the most major brake pad material in Japan, contains almost no steel material. However, because of the cast iron component of the rotor (mating material), Fe is the most abundant metal in brake wear $PM_{2.5}$ (Hagino et al., 2016; Hagino, 2020). The assumptions for Fe, Cu, and Zn contents in brake wear $PM_{2.5}$ were 22%, 1.5%, and 1.3%, respectively, in this study (Table S3).

The composition of tire wear is mostly organic matter and carbon. Zn, added as a vulcanizing agent, is the most abundant heavy metal in tire wear, accounting for approximately 1% (Smolders and Degryse, 2002; Blok, 2005; Grigoratos and Martini, 2014).

It is nearly impossible to separate primary road wear from other mineral dust deposited on roads (Denier van der Gon et al., 2013). Concrete and asphalt, the main components of road surfaces, are mineral aggregates comprising the crustal components Si, Ca, K, Fe, and Al, whose compositional ratios

vary based on the geological source (Harrison et al., 2021). Resuspended particles consist of all non-exhaust particles (brake, tire, and road wear) and particles from other sources deposited on the road surface (e.g., exhaust gas particles, particles from deicing and gritting, wind-blown dust, and biogenic particles) (Harrison et al., 2021). The road dust sampling on asphalted roads in Portugal contained approximately 2%–5% PM_{10}-Fe and 0.03%-0.3% PM_{10}-Cu and PM_{10}-Zn (Alves et al., 2018). In this study, the assumptions for Fe, Cu, and Zn contents in road wear and resuspension PM were 3%, 0.03%, and 0.1%, respectively (Table S3).

Table 4. Assumptions of the metal content ratio in $PM_{2.5}$ from power plant, vehicle exhaust, brake wear, tire wear, road wear and resuspension used in TMI-Asia/Japan v1.1 development.

g-metal/g-$PM_{2.5}$ in %	Fe	Cu	Zn
Thermal power plant	4.2	0.07	0.3
Vehicle exhaust	0.5 – 0.7[a]	0.03 – 0.06[a]	0.2 – 0.4[a]
Brake wear	22.2	1.5	1.3
Tire wear	0	0	1.0
Road wear and resuspension	3.0	0.03	0.1

a. The values used for different vehicle types (mini passenger car, passenger car, light duty truck, heavy-duty truck, bus, and motorcycle) and subsectors by fuel (gasoline, diesel, and LPG) are indicated.

Figure 4 shows the total annual emissions of the anthropogenic $PM_{2.5}$ total mass, Fe, Cu, and Zn in domain 02 Japan region and reductions by 2050 due to the renewable energy shifting, vehicle electrification, and lightweighting. To summarize, in the 2050R&E&L experiment, Fe and Cu were estimated to be reduced by approximately 19%, Zn by 10%, and $PM_{2.5}$ total mass by 9%. The decisive factor in the difference in these reduction rates is the difference in the brake wear-derived contribution to total emissions. In the 2050R&E&L experiment, brake wear has the largest reduction rate in emission factors than tire and road wear and resuspension due to the double effect of the regenerative brake and lightweighting of BEVs. Therefore, the emissions of Fe and Cu, which heavily depend on brake wear, were most significantly reduced.

Renewable energy shifting contributed the most to the reduction of primary $PM_{2.5}$ emissions (−5.8%) (Figure 4a). With the electrification of passenger cars without lightweighting (2050R&E−2050R), the decrease in $PM_{2.5}$ from brake wear and exhaust gas would be partially offset by the increase in $PM_{2.5}$ from tire wear, road wear, and resuspension. As a result, the net reduction in $PM_{2.5}$ emissions was −1.4%, although it did not increase. Lightweighting prevents the increase in tire wear, road wear, and resuspension, further reducing $PM_{2.5}$ emissions by 1.9%. However, passenger car exhaust/non-emission $PM_{2.5}$ accounts for approximately only 10% of total emissions, and in any case, the $PM_{2.5}$ reduction effect of electrification and lightweighting is limited (−3.2%).

611 The largest sources of Fe emissions in Japan are brake wear and the steel industry (included in
612 Industry and others). When $PM_{2.5}$ from brake wear is reduced by 45% by passenger car electrification and
613 lightweighting (Table 1), it contributes to a 9.7% reduction in total Fe emissions. When $PM_{2.5}$ from
614 thermal power plants is reduced by 82% by renewable energy shifting (Table 1), it contributes to an 8.2%
615 reduction in total Fe emissions. As a result, reductions in brake wear and thermal power plants
616 contributed roughly equal to the reduction in Fe emissions (−18.7 ± 1.4%) in 2050 (Figure 4b).
617 Cu emissions from power plants and other sources are relatively low. Brake wear is the largest
618 source of Cu emissions, accounting for 60% of total emissions. Therefore, the reduction in Cu emissions
619 in 2050R&E&L (−18.9 ± 1.8%) is mostly due to the reduced brake wear (−15.4%) due to passenger car
620 electrification and lightweighting (Figure 4c).
621 Zn is characterized by having a tire wear-derived source. In the case of passenger car electrification
622 without lightweighting (2050R&E−2050R), Zn emissions increase from tire and road wear and
623 resuspension (+0.3%) but decrease more from brake wear (−4.0%), resulting in a net decrease (−3.5%)
624 (Figure 4d).
625 The error bars in Figure 4 show the range of lightweight technology progress. The uncertainties are
626 estimated to be ±0.6%, ±1.4%, ±1.8%, and ±0.7% of the $PM_{2.5}$ total mass, Fe, Cu, and Zn emissions in the
627 2050 R&E&L experiment, respectively, which are relatively small. Therefore, from now on, the
628 lightweight technology progress is discussed in terms of low and high averages.
629

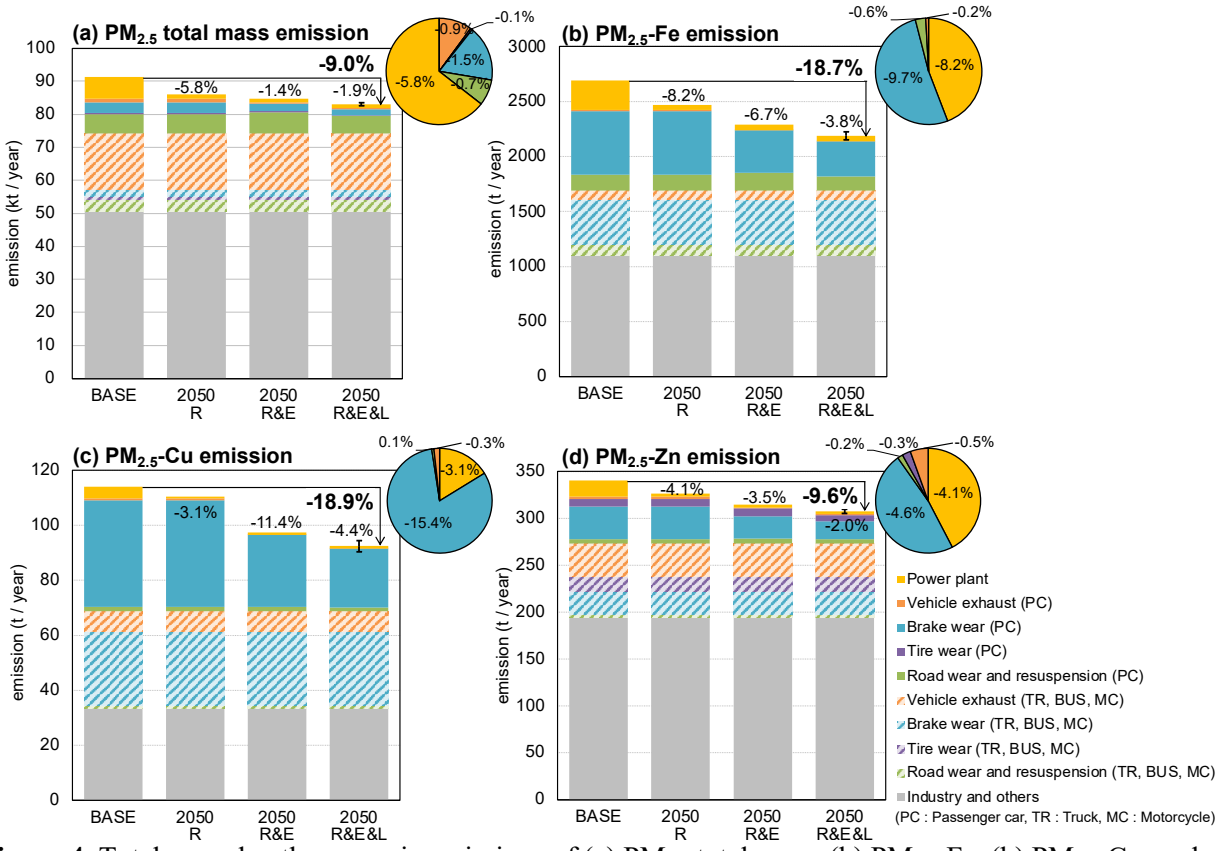

Figure 4. Total annual anthropogenic emissions of (a) $PM_{2.5}$ total mass, (b) $PM_{2.5}$-Fe, (b) $PM_{2.5}$-Cu, and (c) $PM_{2.5}$-Zn in domain 02 Japan region. Comparison between the BASE experiment and each sensitivity experiment. The contributions of sectors to the reduction ratio in the 2050R&E&L case are indicated as a pie chart. The error bars indicate the uncertainty due to the degree of the technological progress of lightweighting; high and low (Figure 2). The reduction ratio shown for each sensitivity experiment represent is based on the BASE experiment. (a) $PM_{2.5}$ emission is based on the PM2.5EI inventory. In this study, the "road dust (including brake wear)" of the original PM2.5EI was allocated to "brake wear" and "road wear and resuspension" in the ratio of 0.35/0.65 (Section 2.1). (b–d) $PM_{2.5}$ metal emissions are based on TMI-Japan, but it does not consider "road wear and resuspension". "Industry and others" sector include aviation, navigation, railway, domestic, cooking, incineration, and field burning.

3.2.1.2. Gaseous pollutants

Figure 5 shows the primary emissions of SO_x, NO_x, and NH_3 in domain 02 Japan region. In the 2050R&E&L experiment, they were reduced by 7%, 16%, and 7%, respectively, in comparison to the base experiment.

The reduction in SO_x emissions is almost entirely due to the reduction in thermal power generation (Figure 5a). The limit of sulfur content in fuel is lower than 0.001% in Japan (CEC, 2003) to maintain the performance of diesel particulate filters (DPFs), so there is originally almost no emission from vehicles.

Both passenger cars and thermal power plants contribute to the reduction of NO_x emissions, while the latter contributes more (−9.8%). The domestic NO_x emissions would only be reduced by −6.1% (Figure 5b), even in the case of a 70% emission reduction due to the passenger car electrification in 2050 (Table 1), because of the high contribution of heavy-duty diesel vehicles.

NH_3 emission reductions were mainly brought by vehicles. NH_3 is generated in power plants during the denitration process and from vehicles as a byproduct of selective catalytic reduction in diesel vehicles and three-way catalysts in gasoline vehicles. The change in energy and vehicles contributed to 1.1% and 5.5% NH_3 emission reductions from the base year in 2050, respectively (Figure 5c).

NMVOC is a precursor of O_3, and O_3 and OH radicals originating from O_3 contribute to the oxidation of NO_x and SO_x to HNO_3 and H_2SO_4, and O_3 and H_2O_2 oxidize SO_2 to produce SO_4^{2-} in liquid water droplets. NMVOC emission decreased by 2% in July and 7% in December due to lower vehicle exhaust emissions and fuel evaporation at fueling stations (figure omitted).

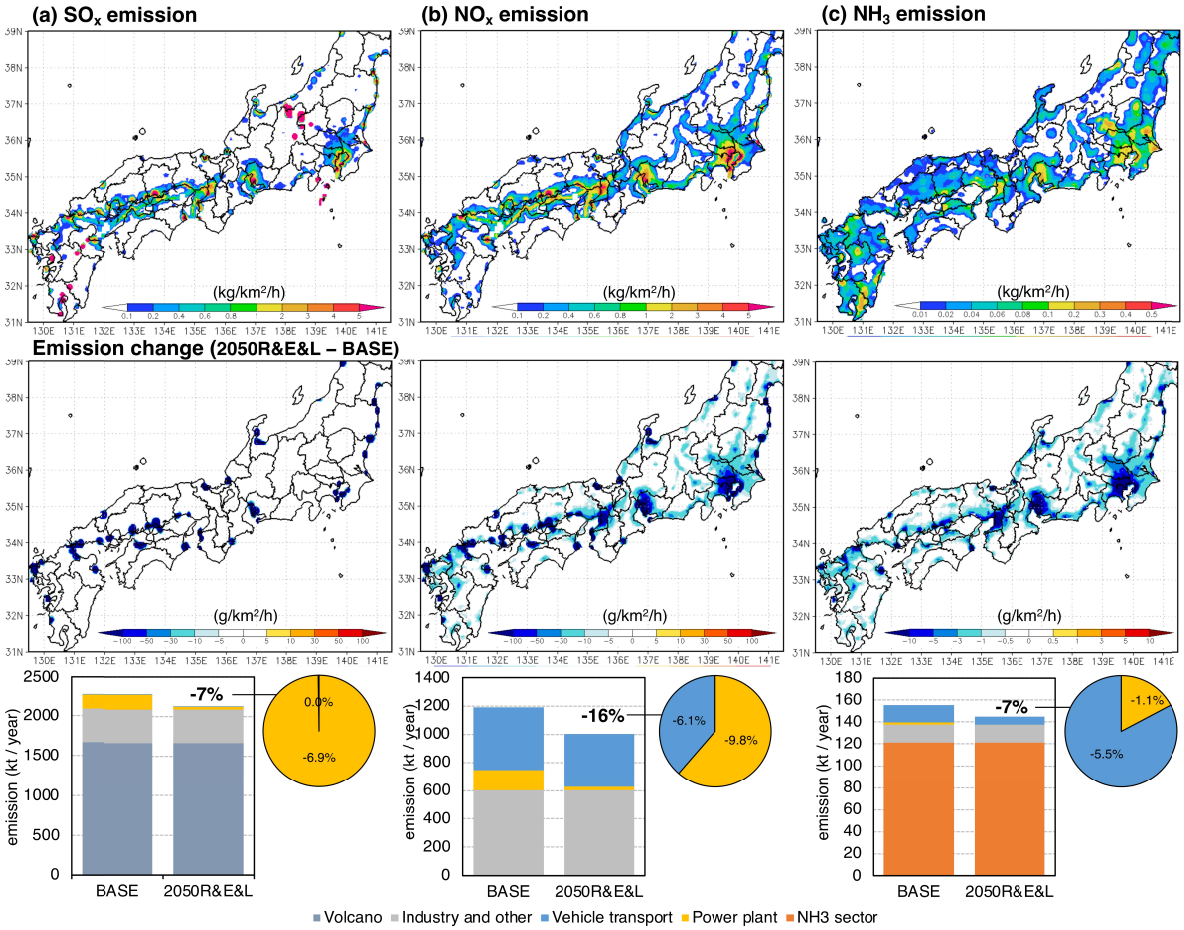

Figure 5. Total annual emissions of (a) SO_x, (b) NO_x, and (c) NH_3 in domain 02 Japan region (top), and reduction in the 2050R&E&L experiment (middle). The bar graphs show the breakdown of the total domestic emission in the BASE experiment and the 2050R&E&L experiment. The contribution of the sectors to the reduction rate is shown as a pie chart. "Industry and other" includes aviation, navigation, domestic, cooking, incineration and field burning. "NH_3 sector" includes livestock, agriculture, and drainage.

3.2.2. Impact on atmospheric $PM_{2.5}$ and $PM_{2.5}$-metals concentration

Figure 6a shows the annual average $PM_{2.5}$ total mass concentration in the BASE experiment, and Figure 6b shows the sensitivity in the 2050 R&E&L experiment. Figure 6c shows the breakdown of $PM_{2.5}$ components in area A (urban area including Tokyo; Figures 6a and 6b black boxes) for each sensitivity experiment. In the 2050R&E&L experiment, the $PM_{2.5}$ concentration was reduced by 8.3% in area A (Figure 6b and 6c).

In area A, renewable energy shifting (2050R–BASE) reduced secondary-formed $PM_{2.5}$ (nitrate and sulfate) more than primary emission-derived $PM_{2.5}$ (i.e., UID, BC, and OC) (Figure 6c). The reduction of SO_x from the thermal power plant freed cations (NH_4^+, Na^+, and Mg^{2+}) in sulfate, which reacted with HNO_3 to form nitrate, thus increasing Na^+ (i.e., the reduction of NO_3^- was probably partially offset). The electrification of passenger cars (2050R&E–2050R) reduced exhaust-derived nitrate and non-exhaust-derived UID by about the same amount (Figure 6c). While the reduction of the $PM_{2.5}$ concentration by the electrification of passenger cars alone is –2.3%, the reduction in non-exhaust PM due to lightweighting (2050R&E&L–2050R&E) increased the effect by more than twice (–5.8%).

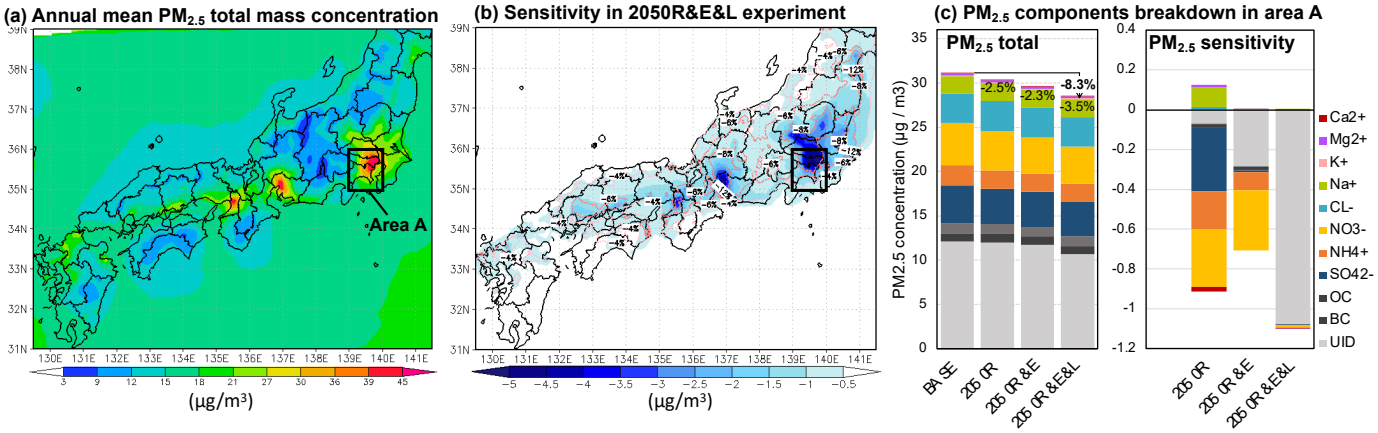

Figure 6. (a) Annual mean concentration of $PM_{2.5}$ total mass in the BASE experiment and (b) sensitivity of the $PM_{2.5}$ concentration in the 2050R&E&L experiment. (c) shows the breakdown of $PM_{2.5}$ components in area A (139–140°E, 35–36°N; urban area including Tokyo).

Figure 7a–7c shows the annual mean concentrations of Fe, Cu, and Zn in $PM_{2.5}$ in the BASE experiment. The concentrations are high in urban areas in the Kanto, Kansai, and Chubu regions, which are major emission sources. For Fe and Zn, the concentration gradient between the Japan Sea and the Japanese Islands is more gradual than that for Cu, suggesting a relatively higher contribution from continental transport. As a result of source–receptor analysis, the contribution of the emissions from the Asian continent was high for Zn, Fe, and Cu in that order, and the seasonal variations associated with continental advection (high concentrations in winter and spring, low concentrations in summer) were

distinct in the same order (Figure S11). The effect of reducing domestic emissions was higher in the summer months when the continental contribution was lower for all metals.

In the 2050R&E&L experiment, Fe, Cu, and Zn concentrations were reduced by 13%, 18%, and 5%, respectively, in area A (Figure 7d–7f). The rate of primary emission reduction for Fe and Cu was similar at –19% (Figure 4b and 4c), but Cu reduced the concentration more. This may be because brake wear was the dominant contributor to the primary emission reduction of Cu, effectively reducing the areal concentration. For Fe, the contribution of power plants to emission reductions was higher than for Cu, indicated by more localized reductions in concentrations near coastal thermal power plants in East Japan (Figure 7d).

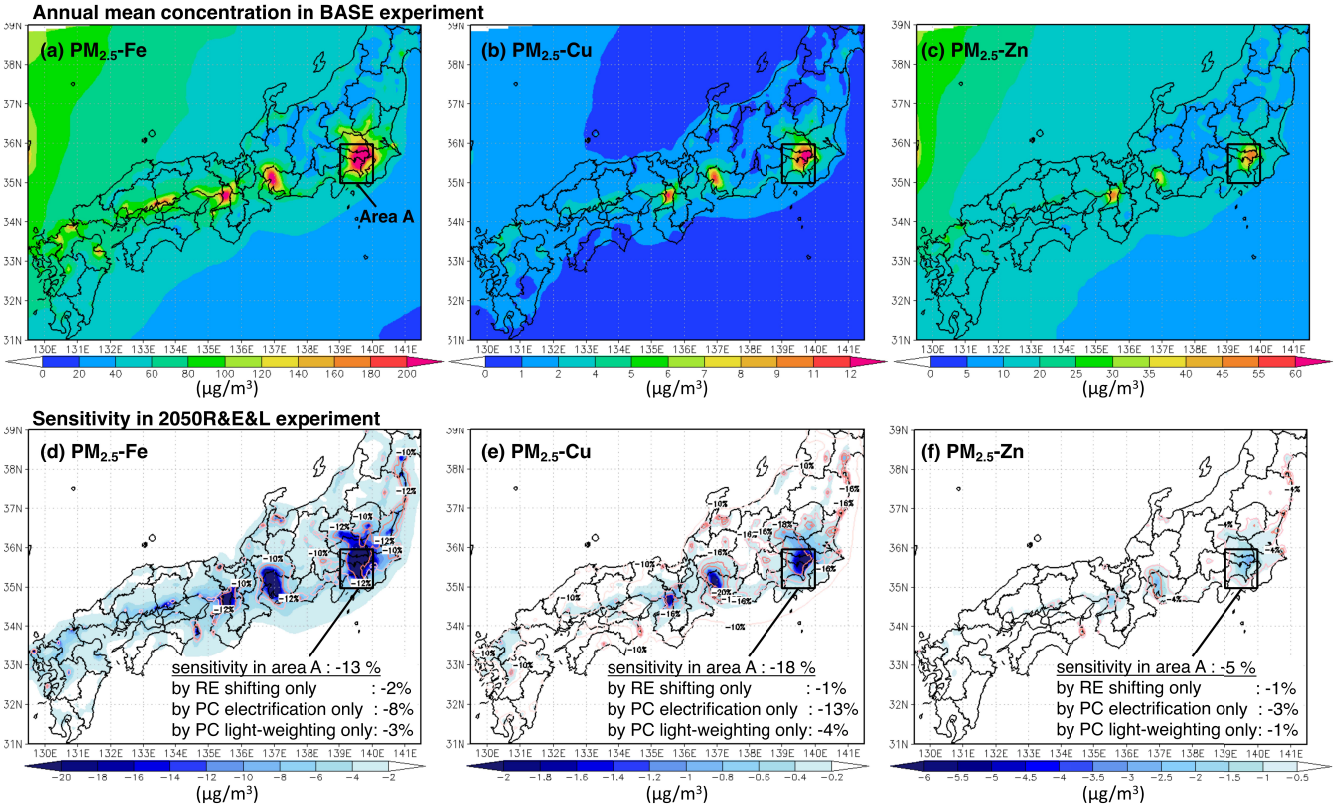

Figure 7. Annual mean concentrations of (a) $PM_{2.5}$-Fe, (b) $PM_{2.5}$-Cu, and (c) $PM_{2.5}$-Zn in the BASE experiment. (d–f) are the sensitivity of (a–c) in the 2050R&E&L experiment. The sensitivity in area A and that due to renewable energy (RE) shifting, passenger car (PC) electrification, and PC lightweighting alone are shown in the figure d–f. As in Figure 6, the urban area is enclosed as area A (139–140°E, 35–36°N).

3.2.3. Impact on aerosol acidity

Figure 8 shows the monthly mean aerosol pH in July and December. July and December were chosen because pH is generally lower in summer and higher in winter. The main reason for the low pH during the summer months is the high concentration of oxidants due to high solar radiation, which promotes sulfate formation (Guo et al., 2018; Song and Osada, 2020). NH_4^+ and NO_3^- migrate to the gas phase at high temperatures, while SO_4^{2-} is always in the particulate phase due to its low vapor pressure. The loss of NH_4^+ from NH_4NO_3 and $(NH_4)_2SO_4$ predominates over the loss of NO_3^- only from NH_4NO_3, and the net increase in particle H^+ lowers pH (Guo et al., 2018). The pH was estimated to range from 0.5 to 1.5 in July and from 1 to 3 in December in this study.

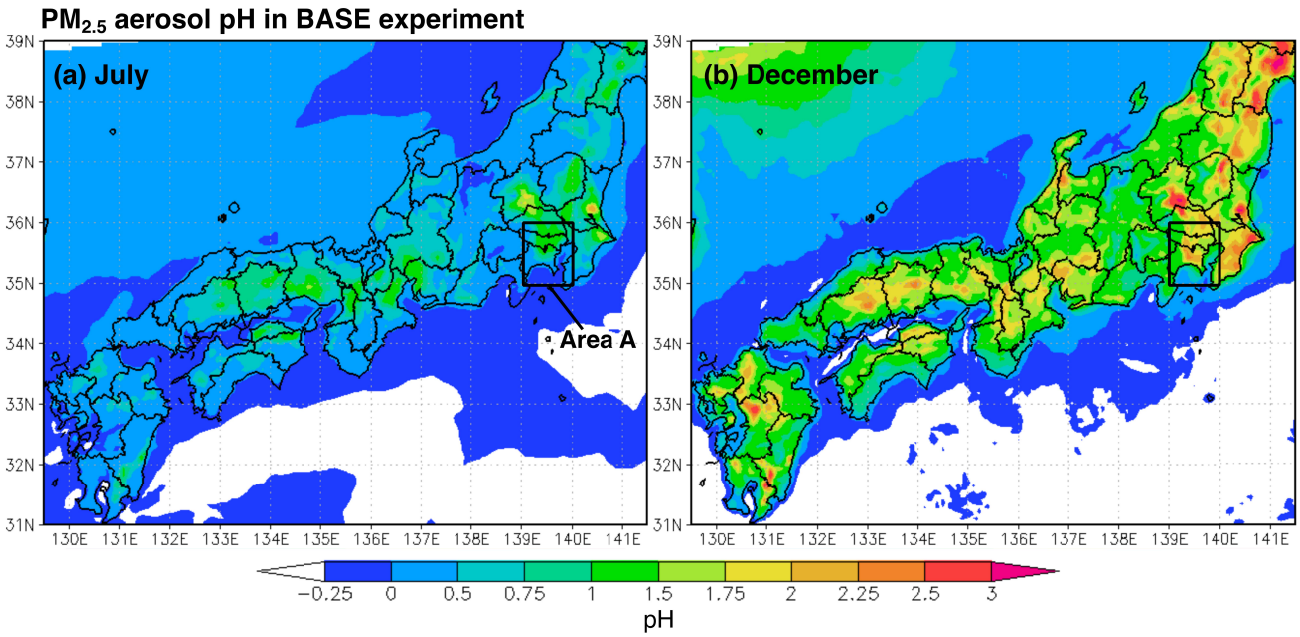

Figure 8. Simulated monthly mean of $PM_{2.5}$ aerosol pH in (a) July and (b) December in the BASE experiment, averaged using only hourly data of 20% < RH < 95%. As in Figure 6, the urban area is enclosed as area A (139–140°E, 35–36°N).

Figure 9a shows the change in aerosol pH in July in the R&E&L experiment. Figure 9b, 9e, and 9h show the sensitivity by renewable energy shifting, passenger car electrification and lightweighting alone, respectively. The results for December are also shown in Figure S17. Aerosol pH depends both on H^+_{air} and LWC concentration. Acidic substances such as H_2SO_4 and HNO_3 increase H^+_{air}, while basic substances such as NH_3 decrease H^+_{air} in aerosols (hereafter referred to as the H^+_{air} process). The increase in water-soluble aerosols increases the LWC and decreases the pH (hereafter referred to as the LWC

process). The net pH sensitivity (ΔpH_{NET}) is equal to the sum of the pH sensitivity of the H^+_{air} process alone (ΔpH_{H^+}) and that of the LWC process alone (ΔpH_{LWC}).

The respective sensitivities can be derived by Equations (5)–(7):

$$\Delta pH_{NET} = -\log_{10}\left(\frac{1000\gamma_{H^+}\cdot H^+_{air\,sens}}{LWC_{sens}}\right) + \log_{10}\left(\frac{1000\gamma_{H^+}\cdot H^+_{air\,cntrl}}{LWC_{cntrl}}\right) \quad (5)$$

$$\Delta pH_{H^+} = -\log_{10}\left(\frac{1000\gamma_{H^+}\cdot H^+_{air\,sens}}{LWC_{cntrl}}\right) + \log_{10}\left(\frac{1000\gamma_{H^+}\cdot H^+_{air\,cntrl}}{LWC_{cntrl}}\right) \quad (6)$$

$$\Delta pH_{LWC} = -\log_{10}\left(\frac{1000\gamma_{H^+}\cdot H^+_{air\,cntrl}}{LWC_{sens}}\right) + \log_{10}\left(\frac{1000\gamma_{H^+}\cdot H^+_{air\,cntrl}}{LWC_{cntrl}}\right) \quad (7)$$

where $H^+_{air\,cntrl}$ and LWC_{cntrl} are the reference H^+_{air} and LWC concentrations (μg m^{-3}), and $H^+_{air\,sens}$ and LWC_{sens} are those of sensitivity. The renewable energy shifting decreased aerosol acidity (maximum pH +0.2) in areas near power plants (Figure 9b), and the passenger car electrification increased aerosol acidity (maximum pH –0.2) in urban areas (Figure 9e). The aerosol acidity increased slightly net in urban areas in 2050 (maximum pH –0.1) (Figure 9a).

The explanation of the sensitivity of pH due to renewable energy shifting is relatively simple. Renewable energy shifting mainly reduces SO_x and NO_x emissions from power plants but has a small effect on NH_3 reduction. Also, because SO_4^{2-} is nonvolatile, the effect on pH due to the SO_x emission control is not affected by gas–aerosol distribution, contrary to the case of NO_x and NH_3 emission control. Therefore, ΔpH_{H^+} increased (Figure 9c). Although the LWC decreases as SO_4^{2-} decreases, the freed cations (such as NH_4^+ and Na^+) form nitrate with HNO_3 (Seinfeld and Pandis, 2016), which may partially offset the LWC decrease. Despite the reduction in power plant NO_x emissions, increases in nitrate partially occurred in this study as well, but the effect of sulfate reduction was larger, resulting in a net decrease in LWC (ΔpH_{LWC} decrease) (Figure 9d). Finally, the effect of H^+ reduction (pH increase) (Figure 9c) was greater than the effect of concentration by LWC reduction (pH decrease) (Figure 9d), resulting in a net pH increase (Figure 9b).

The vehicle electrification contributed to the pH decrease (Figure 9e). The reduction of on-road NO_x and NH_3 resulted in an increase in H+ (ΔpH_{H^+} decreased) in urban areas in July as a result of the acid–base balance (Figure 9f). However, in December, unlike the trend in July, the distribution of ΔpH_{H^+} was random with mixed positive and negative values (Figure S17f). These differences in sensitivity trends are due to seasonal differences in aerosol pH. The aerosol pH was lower in summer, and NH_4^+ tended to be more present in the particle phase than NO_3^-, so NH_3 emission reduction was effective in reducing NH_4^+ (i.e., increasing H^+) in the particle phase. This mechanism of seasonal differences in aerosol pH sensitivity due to NO_x and NH_3 emission controls is discussed in detail in Appendix A. The effect of ΔpH_{LWC} was small in both summer and winter (Figure 9g).

758 The vehicle lightweighting had little effect on either the H^+ or LWC process (Figure 9i and 9j). Note
759 that the impact of light-weighting alone is due only to reduced fuel evaporative NMVOC emissions at the
760 gas station and not to any change in on-road emissions (Table 1).
761

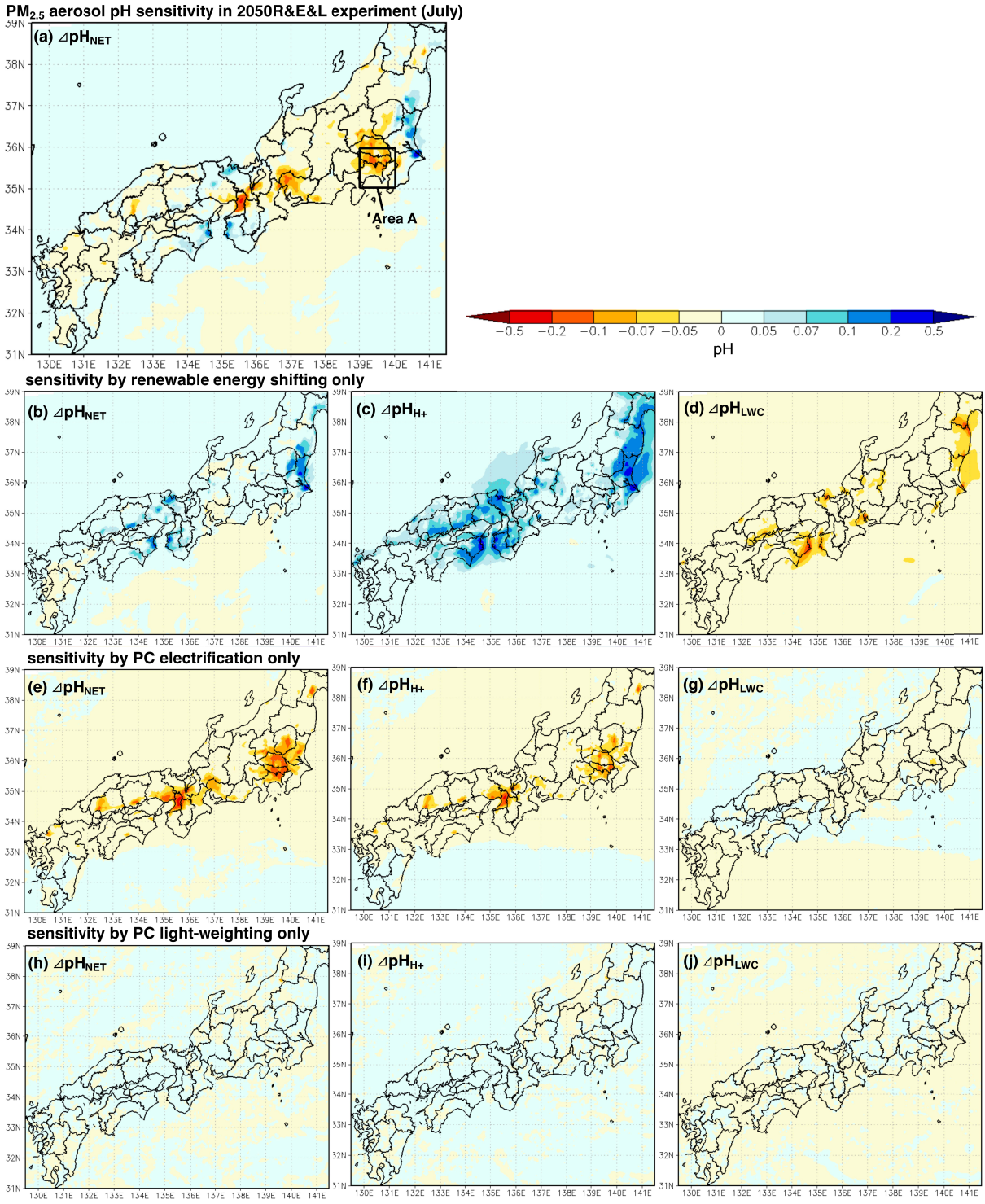

Figure 9. (a) $PM_{2.5}$ aerosol pH sensitivity in the R&E&L experiment in July. Rows 2, 3, and 4 are the aerosol pH sensitivity by (b) renewable energy shifting, (e) passenger car (PC) electrification, and (h) PC lightweighting alone, respectively. The sum of ΔpH_{H^+} (center) and the ΔpH_{LWC} (right) is ΔpH_{NET} (left). The ΔpH_{H^+} is the effect of the H^+ process, that is sensitivity in the amount of hydronium ions due to change in acidic or basic substances (c, f, i). The ΔpH_{LWC} is the effect of the LWC process, which is the change in aerosol water content due to the change in the mass of water-soluble aerosols (d, g, and j). As in Figure 6, the urban area is enclosed as area A (139–140°E, 35–36°N).

3.2.4. Impact on water-soluble metals

Finally, the sensitivity of water-soluble metal concentrations is discussed, considering the water solubility of metals depending on aerosol pH. Figure S18 shows the relationship between aerosol pH and the water solubility of Fe and Cu indicated by Fang et al. (2017). The solubility of metals increases significantly below pH 2–3 (Fang et al., 2017; Wong et al., 2020). Fang et al. (2017) did not measure Zn, but Zn was reported to have a higher water-soluble fraction under the same pH conditions than Cu (Shahpoury et al., 2021), and in this study we assumed that the water-soluble fraction of Zn is the same as that of Cu.

The change in metal solubility due to emission changes in 2050 (2050R&E&L–BASE) was estimated to be negligible (<1%). Note that the uncertainties in the NO_3^- concentration and RH of the model simulations may result in biases less than ±1% and ±3% for changes in the water-soluble fractions of Fe and Cu, respectively. In addition, water-soluble fractions may be affected by history in past transport pathways (Wong et al., 2020), but this effect was not considered. In addition, the solubility of metals is promoted by not only changes in aerosol pH (i.e., proton-driven) but also by complex formation with organic materials and their photoinduced dissolution. The solubility of Fe at pH 2 with oxalate under dark conditions was found to be four times greater than that of proton-promoted dissolution, and photoinduced dissolution was twice greater than that found under dark conditions based on laboratory experiments (Chen and Grassian, 2013; Ito, 2015). The effects of such ligand-drive and photoinduced dissolution were not considered in this analysis. Compared to the ranges of these uncertainties and the seasonal variation of aerosol pH, the sensitivity of metal solubility in the 2050R&E&L experiment was estimated to be very small.

Table 5 summarizes the total metal concentrations, water-soluble fractions of metals, and water-soluble metal concentrations in area A. Their respective spatial distributions are shown in Figure S19. The sensitivity of water-soluble metal concentrations in the 2050R&E&L experiment depends on (1) changes in primary metal emissions and (2) changes in aerosol acidity, and sensitivity due to each alone is also shown. As described above, aerosol acidity is largely determined by seasonality. The sensitivity of water-soluble metal concentrations depends on (1) changes in primary metal emissions and is barely by (2) changes in aerosol acidity (maximum +2% for Fe and maximum +0.5% for Cu and Zn). Therefore, the primary emission control of metals is more important than gaseous pollutants in reducing water-soluble metal concentrations.

Table 5. Total metal concentrations, water-soluble fractionss of metals and water-soluble metal concentrations in area A (139–140°E, 35–36°N). Comparison of the BASE and 2050R&E&L experiments for water-soluble metal concentrations and the contribution to these from (1) changes in primary metal emissions and (2) changes in aerosol acidity alone, respectively.

		total metal concentration (ng m^{-3})	water-soluble fraction of metals[a] (%)	water-soluble metal concentration (ng m^{-3})		water-soluble metal sensitivity (ng m^{-3})	
				BASE	2050R&E&L (sensitivity from BASE in %)	(1) by metal emission change	(2) by aerosol acidity change
July	Fe	147.0	34	49.5	43.8 (–12%)	–6.8 (–14%)	+1.0 (+2%)
	Cu	6.1	100	6.1	5.0 (–18%)	–1.1 (–18%)	±0.0 (±0%)
	Zn	19.8	100	19.8	19.0 (–6%)	–1.2 (–6%)	±0.0 (±0%)
December	Fe	169.3	12	20.0	20.1 (–9%)	–2.4 (–11%)	+0.5 (+2%)
	Cu	7.3	52	3.7	3.2 (–17%)	–6.0 (–17.5%)	+0.02 (+0.5%)
	Zn	30.3	52	15.8	15.5 (–4%)	–0.7 (–4.5%)	+0.1 (+0.5%)

a. The water-soluble fraction of metals was derived from the calculated aerosol pH and Figure S18 (relationship between aerosol pH and the water-soluble fraction of metals indicated by Fang et al. (2017)). Since there is no information on the water-soluble fraction of Zn, it was assumed to be the same as that of Cu.

4. Conclusions and Future issue

The impacts of renewable energy shifting, passenger car electrification, and lightweighting on the atmospheric concentrations of the $PM_{2.5}$ total mass, Fe, Cu, and Zn and aerosol acidity in Japan through 2050 were evaluated using a regional meteorology–chemistry model.

The domestic primary emissions of $PM_{2.5}$, Fe, Cu, and Zn reduced by 9%, 19%, 18%, and 10%, and their surface concentrations in the urban area decreased by 8%, 13%, 18%, and 5%, respectively. On a $PM_{2.5}$ mass basis, BEVs have been considered to have no advantage in non-exhaust PM emissions because the increased tire and road wear and resuspension due to their heavy weight offset the benefit of brake wear reduction by the regenerative brake. Indeed, passenger car electrification without lightweighting also did not significantly reduce the $PM_{2.5}$ concentration in the urban area in this study (–2%) but was highly effective in reducing Fe and Cu concentrations owing to high brake wear-derived contributions (–8% and –13%, respectively). In addition, this study estimated that the lightweighting of the drive battery and the body frame would reduce even tire and road wear and resuspension. Therefore, vehicle electrification (mainly BEVs) and lightweighting could be one of the effective means of reducing the risk of respiratory inflammation.

Renewable energy shifting reduced SO_x and NO_x emissions from thermal power plants and decreased aerosol acidity near power plants (maximum pH +0.2), while the passenger car electrification reduced NO_x and NH_3 emissions and slightly increased aerosol acidity in the urban are as a result of acid–base balance (maximum pH –0.2). It is because that, in summer, NH_4^+ tends to be more present in the particle phase than NO_3^- due to the low pH of the aerosol and NH_3 emission reductions were more effective than NO_x reductions on aerosol acidity. In winter, their effects were comparable. However,

anyway, changes in aerosol acidity little changed water-soluble metal concentrations (maximum +2% for Fe, +0.5% for Cu, and Zn); therefore, it is important to reduce primary metal emissions.

Finally, we present four major future issues for the model prediction of the risk of respiratory inflammation due to air pollutants.

1. Consideration of PAHs and PAH quinones in the model. PAH quinones catalytically consume DTT in the redox cycle (Kumagai et al., 2002; Jiang et al., 2019; McWhinney et al., 2013; Charrier and Anastasio, 2012) and also have noncatalytic DTT-consuming effects through direct addition with DTT (Gant et al. al., 1988; Katritzky et al., 2008). PAHs are also reduced to quinones in the body by reductases such as cytochrome P-450 (Kumagai et al., 2012; Jiang et al., 2019).
2. Consideration of the source-dependent solubility of metals. The Fe solubility of pyrogenic aerosols such as biomass burning and fossil fuel combustion varies greatly depending on the source and can be one to two orders of magnitude higher than that of lithogenic aerosols (as low as 0.5%) (Ito et al, 2021). Oakes et al. (2012) estimated Fe solubility in automobile exhaust and biomass burning to be 51–75% and 46%, respectively. The solubility of aerosol Fe in coal fly ash (present as glassy Fe (oxyhydroxide aggregates)) was reported to be less than 1%, while the that of oil fly ash (present as ferric sulfate salt) was as high as 36% (Desboeufs et al., 2005) and even approximately 80 % (Schroth et al., 2009). In metal modeling, it is ideal to be able to set the initial solubility rate at primary emissions linked to emission inventories, in addition to the atmospheric process of changing solubility due to protons and ligands.
3. Consideration of organic matter in the model. Water-soluble organic compounds (WSOCs) such as HULIS and transition metals have synergistic, additive, or antagonistic effects on OP_{DTT} (Xiong et al., 2017; Yu et al., 2018; Lin and Yu, 2020). WSOCs also contain atmospheric ROS (H_2O_2, ROOH), which decompose in the body to bring OH radicals (Tong et al., 2016). Furthermore, the complex formation of metals with the organic ligands of oxalates solubilizes the metals (Chen and Grassian, 2013; Zhou et al., 2015; Wong et al., 2020). Ligand-driven iron dissolution may play an important role, especially under low-pH conditions, compared to proton-driven dissolution (Chen and Grassian, 2013). This is because under high pH conditions, the Fe particle surface loses its positive charge, while the acid dissociates and becomes more negatively charged, resulting in a repulsive electrostatic action that makes it less likely for the acid to approach and bind to the surface (Chen and Grassian, 2013; Miller et al., 1986). Therefore, it is important to consider the organic matter in terms of its own ROS-producing capacity and metal solubilization.
4. Consideration of differences in metal solubility between the atmosphere and the body. Because the respiratory tract is water-saturated and the alveolar epithelial lining fluid is weakly basic, the

865 solubility of metals that affects ROS production may be different between the atmosphere and the
866 body, requiring further investigation.
867 5. Improvement of the reproducibility of nitrate concentration by NHM-Chem. The current NHM-Chem
868 was found to overestimate NO_3^- especially in the summer, due probably to the overestimation of the
869 $PM_{2.5}$ fraction of sea salt particles (to produce $NaNO_3$). This overestimation does not substantially
870 affect the main results of this study, but should be resolved in the future using size-resolved
871 measurements of inorganic compounds.
872

Appendix A. Effect of gas–aerosol partitioning on nitrate sensitivity to NO_x and NH_3 emission control

As described in Section 3.2.3, on-road NO_x and NH_3 emission changes due to passenger car electrification alone increased H^+ (decreased pH) in urban areas in July, while the sensitivity was random in December (Figure A1). Reducing NO_x and NH_3 will not affect aerosol pH if HNO_3 and NH_3 gases are reduced, not the particle phase. Therefore, this seasonal difference in sensitivity is discussed in terms of the gas–aerosol partitioning of HNO_3–NO_3^- and NH_3–NH_4^+.

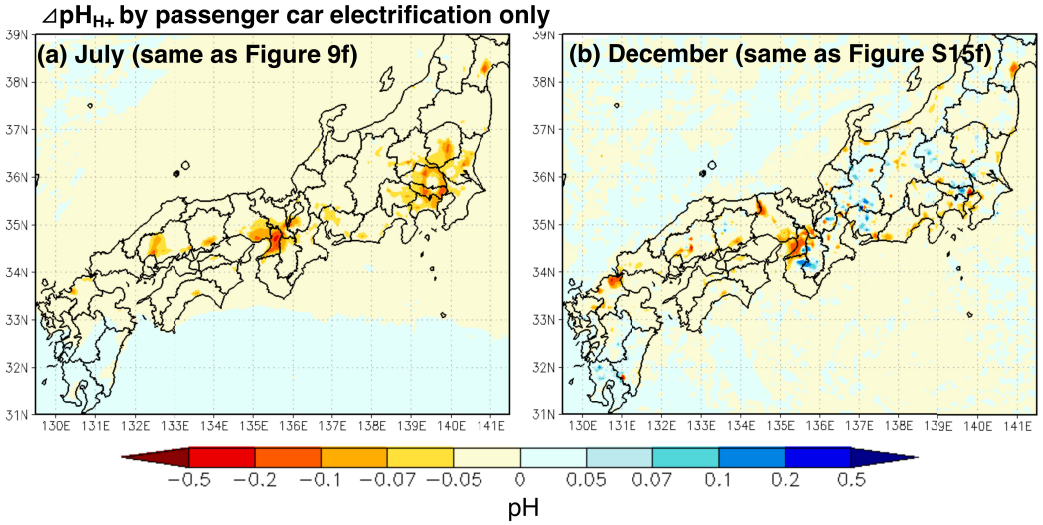

Figure A1. Change in ΔpH_{H^+} due to passenger car electrification only. Same as Figures 9f and Figure S15f for (a) July and (b) December, respectively.

Figure A2 shows the ratio of concentration sensitivity based on passenger car electrification alone. In December, the reduction ratios of the molar concentrations of NH_4^+ and NO_3^- were comparable (1 to 1.1 times), while in July, NH_4^+ was reduced more than 2 times than NO_3^- in many areas (Figure A2a). The ratio of the particle phase (NH_4^+) reduction to the total ammonium ($TNH_4 = NH_4^+ + NH_3$) reduction was comparable in July and December (Figure A2b), whereas for total nitric acid ($TNO_3 = NO_3^- + HNO_3$), the reduction was clearly more from the particle phase (NO_3^-) in December than in July (Figure A2c). This means that NO_3^- in the particle phase was less reduced in July than in December, and NH_4^+ was reduced more than NO_3^- from the particle phase. The equilibrium constants for $NH_3 + H^+ \rightarrow NH_4^+$ and $HNO_3 \rightarrow NO_3^- + H^+$ ($H^*_{NH_3}$ and $H^*_{HNO_3}$, respectively) decrease faster for $H^*_{NH_3}$ than for $H^*_{HNO_3}$ with increasing temperature (Guo et al., 2018; Clegg et al.,1998; Clegg and Brimblecombe, 1990). Therefore, during high temperatures in the summer, NH_4^+ is more likely to remain in the particle phase than NO_3^-. Nevertheless, NH_4^+ was reduced more, likely due to the low aerosol pH in July. The reasons are described in detail below.

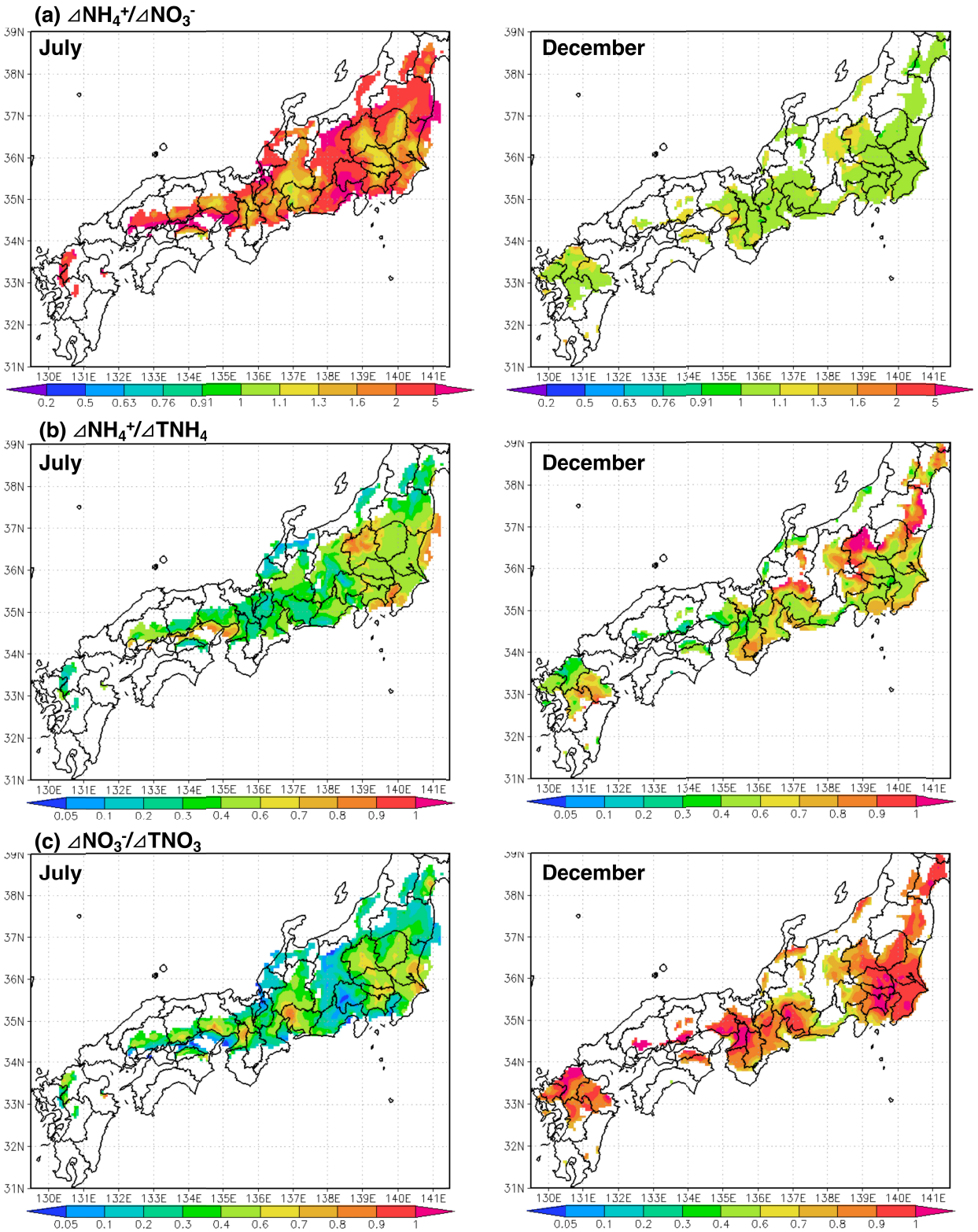

Figure A2. (a) Reduction ratios of NH_4^+ and NO_3^- concentrations ($\Delta NH_4^+/\Delta NO_3^-$) by passenger car electrification only (2050R&E–2050R), (b) ratio of NO_3^- in the reduction of TNO_3 (= NO_3^- + HNO_3), and (c) ratio of NH_4^+ in the reduction of TNH_4 (= NH_4^+ + NH_3). Only the grids with TNO_3 and TNH_4 reduction ratios greater than 5% were drawn.

902 Figure A3 shows the ratio of the particle phase in TNO_3 or TNH_4 ($\varepsilon NO_3 = NO_3^-/(NO_3^- + HNO_3)$,
903 $\varepsilon NH_4 = NH_4^+/(NH_4^+ + NH_3)$, respectively) to ambient aerosol pH conditions. The dots are scatter plots of
904 aerosol pH and εNO3 and εNH4 from the simulation results (2050R experiment). In July, NH_4 is clearly
905 partitioned into the particle phase and NO_3 into the gas phase, and the two are almost completely
906 separated (Figure A3a), whereas, in December, the same trend as described above was observed in the
907 relatively low-pH region (<0.5), but the gas–aerosol partitioning of NO_3 and NH_4 was comparable in most
908 cases, ranging from approximately 0.4 to 0.9 (Figure A3b).
909 Guo et al. (2017) proposed that εNO_3^- and εNH_4^+ can be expressed as sigmoid functions with respect
910 to pH by the following Equations (A1) and (A2), depending on the ambient aerosol pH, LWC, and T
911 conditions.

$$\varepsilon NO_3^- = \frac{K_{n1}\, H_{HNO_3}\, C_w\, R\, T}{\gamma_{H^+}\gamma_{NO_3^-}\, H_{aq}^+ + K_{n1}\, H_{HNO_3} C_w\, R\, T} \qquad (A1)$$

$$\varepsilon NH_4^+ = \frac{\frac{\gamma_{H^+}}{\gamma_{NH_4^+}} \frac{H_{NH_3}}{K_a} H_{aq}^+\, C_w\, R\, T}{1 + \frac{\gamma_{H^+}}{\gamma_{NH_4^+}} \frac{H_{NH_3}}{K_a} H_{aq}^+\, C_w\, R\, T} \qquad (A2)$$

912
913 where H_{aq}^+ is the concentration of hydronium ions in the aerosol aqueous phase (mol L^{-1}), C_w is the LWC
914 in air (μg m^{-3}), K_{n1} and K_a are the acid dissociation constants for HNO_3 and NH_4^+, respectively ($K_{n1} =$
915 12, $K_a = 5.69 \times 10^{-10}$), R is the gas constant, and T is the temperature (K). H_{HNO_3} and H_{NH_3} are
916 Henry's Law constants for HNO_3 and NH_3, which are functions of temperature. γ_{H^+}, $\gamma_{NO_3^-}$, $\gamma_{NH_4^+}$ are the
917 ion activity coefficients of H^+, NO_3^-, and NH_4^+ respectively. $\gamma_{H^+}\,\gamma_{NO_3^-} = 0.324$ and $\gamma_{NH_4^+}\,\gamma_{NO_3^-} = 0.017$,
918 in this study.
919 The S-curves in Figure A3 are εNO_3^- and εNH_4^+ derived from theoretical Equations (A1) and (A2).
920 εNO_3^- increases with higher ambient aerosol pH due to promoted particulation. The S-curve of εNO_3^-
921 shifts to the right as gasification is promoted at higher temperatures and lower humidity, even under the
922 same pH conditions. εNH_4^+, contrary to εNO_3^-, tends to be higher at lower pH and tends to shift to the left
923 at higher temperatures and lower humidity. The gas–aerosol partitioning of the simulation results is
924 consistent with the function derived in the theoretical equation; that is, it can be approximately explained
925 by aerosol pH, LWC, and temperature.
926

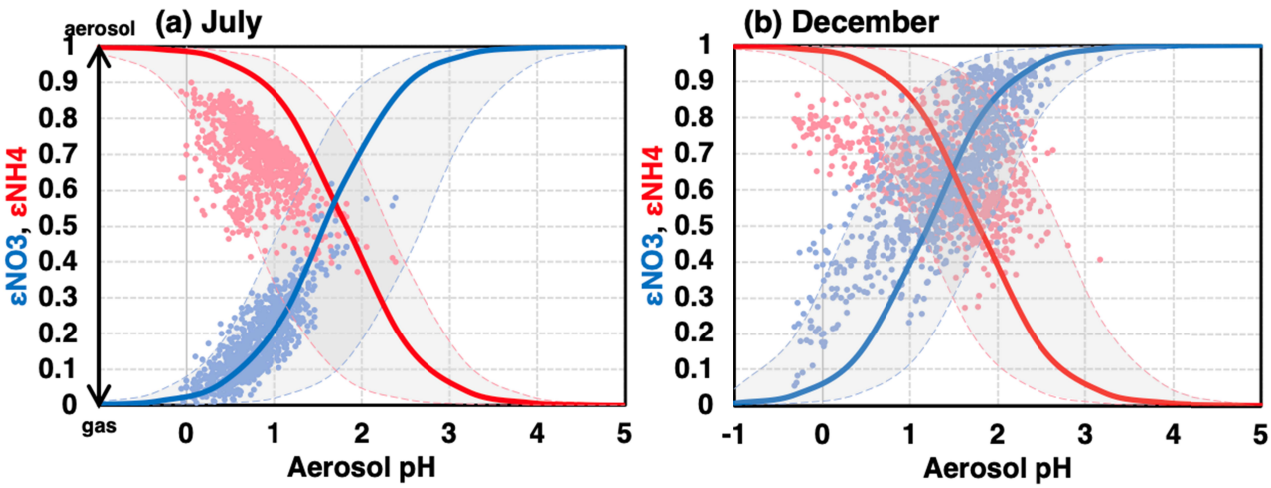

Figure A3. Relationship of εNO_3^- and εNH_4^+ to ambient aerosol pH in (a) July and (b) December. The scatter plots are the results of the model simulation (2050R experiment). Only data from grids that were relatively sensitive (ΔpH_{H^+} >0.05) in Figure A1a and A1b are plotted for the purpose of interpreting their positive and negative sensitivity. The S-curves were derived using the theoretical equation proposed by Guo et al. (2017) shown in Equations A1 and A2, with monthly averages of temperature and LWC for the model grid of interest (July: T = 297 K, C_w = 12.7 μg m^{-3}; December: T = 279 K, C_w = 5.0 μg m^{-3}). The gray shading indicates the max–min temperature range and LWC. These figures were drawn using the spread sheet provided as Supporting information of Nenes et al. (2020).

Nenes et al. (2020) proposed a new framework to evaluate whether NO_x and NH_3 emission controls are effective in reducing particle phase concentrations by a chemical sensitivity window delimited by εNO_3^- and εNH_4^+ thresholds. In Figure A3, it can be considered that controlling primary emissions is not effective in reducing aerosol mass when the particle fraction is low. When the threshold value of εNO_3^- (or εNH_4^+) = 0.3 was used in this study, the pH was uniquely determined from the sigmoid function, and when it is applied to various LWC widths, Figure A4 was obrained. In this way, the four chemical sensitivity windows derived can be classified as 1: NO_x control effective, 2: NH_3 control effective, 3: both NO_x and NH_3 control effective, and 4: NO_x nor NH_3 control ineffective.

In July, most of the target data (model simulation result data for the grid with ΔpH_{H^+} >0.05 in Figure A1) are classified into chemical window 2 (Figure A4a), consistent with the positive trend of ΔpH_{H^+} in Figure A1a. The blue line is located higher in July than in December due to higher temperatures, and NO_x emission control is ineffective, except for higher aerosol pH. However, because of the low aerosol pH in summer (the plot is located lower than in December), many were not classified in chemical window 1 or 3 (Figure A4a). The high humidity and high LWC characteristics of summer make emission controls more effective in reducing particle phase concentrations (the plot is more to the right than in December), and part of the plots was classified as chemical window 3. In the horizontal distribution of chemical windows, the area of no ΔpH_{H^+}sensitivity in Tokyo and Saitama corresponded to chemical window 3 (Figure A5a,

Figure A1a), suggesting that the effects of acid and base reduction due to decreases in both NO_3^- and NH_4^+ were offset.

In December, many of the target data were evaluated to be classified in chemical window 3, and some were classified in windows 1 and 2. This is also consistent with the random trend of ΔpH_{H^+} in Figure A1b. With similar rates of NO_3 and NH_4 as particle phases (Figure A3b), the offsetting effects of NO_3^- and NH4+ reduction occur in many grids. In December, the positive and negative distribution of ΔpH_{H^+}did not correspond to the horizontal distribution of chemical window classification (Figure A5b, Figure A1b). This framework is only a sensitivity classification for aerosol mass, so the classification might be slightly different if the ionization of NO_3^- and NH_4^+ is considered. These results suggested that NO_3 tends to exist in the gas phase and NH_4 in the particulate phase during the summer due to the low pH and that the effect of NH_3 reduction was dominant despite the reduction of both NO_x and NH_3 as a result of the chemical sensitivity window classification.

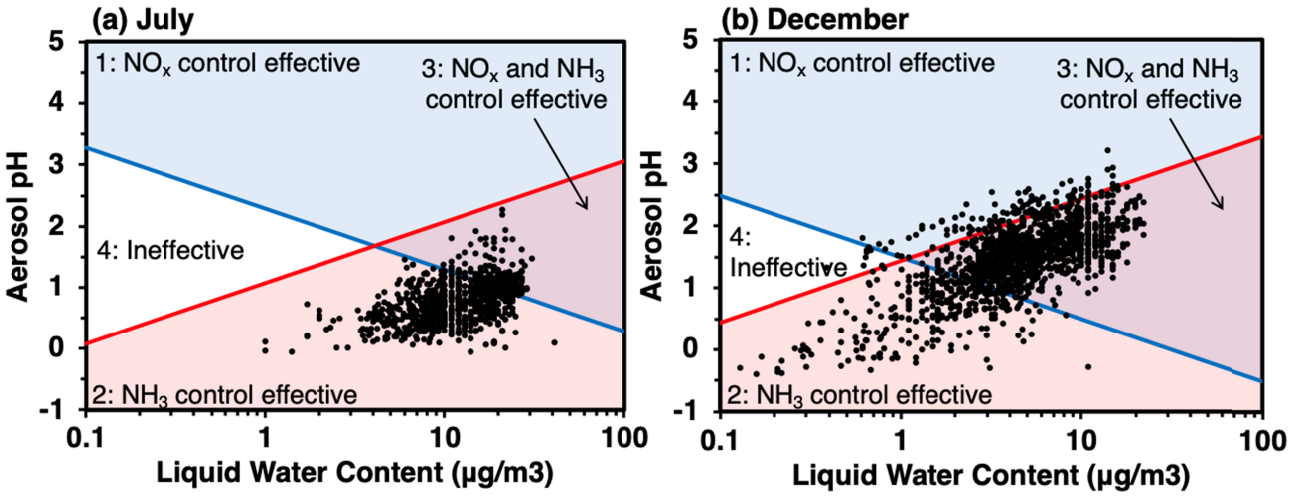

Figure A4. Evaluation of chemical sensitivity windows of the particle phase by NO_x and NH_3 emission control. The effectiveness of NO_x and NH_3 emission control is classified into four "windows" depending on the LWC and aerosol pH conditions. The solid blue (or red) line is the boundary of εNO_3^- (or εNH_4^+) = 0.3 derived by the theoretical equation of Guo et al. (2017) shown in Equations A1 and A2. In the windows where pH is below the blue line or above the red line, NO_3 and NH_4 are relatively abundant in the gas phase (>70%) and NO_x (NH_3) emission control is considered ineffective. The temperatures are the monthly average values (July: T = 297 K, December: T = 279 K). The plots are model simulation result data for the grid with ΔpH_{H^+} >0.05 in Figure A1 and Figure A3. These figures were drawn using the spread sheet provided as Supporting information of Nenes et al. (2020).

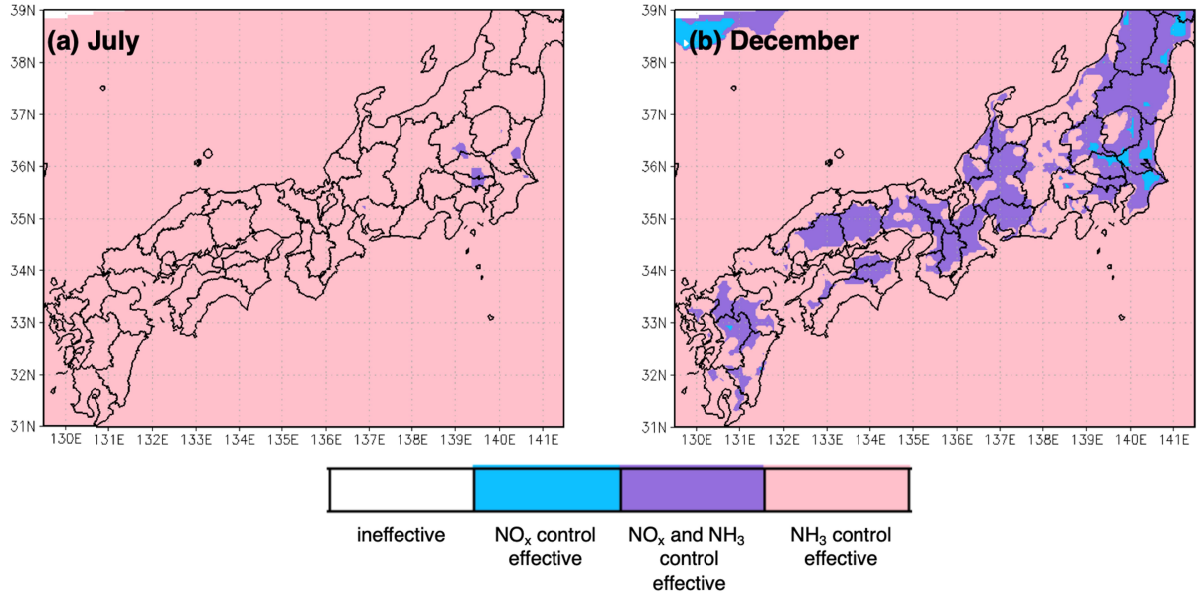

976 **Figure A5.** Horizontal distribution of the chemical sensitivity window classification of the particle phase
977 for NO_x and NH_3 emission control in (a) July and (b) December.
978

Acknowledgments

The authors are thankful for Drs. Tazuko Morikawa and Hiroyuki Hagino of Japan Automobile Research Institute for providing PM2.5EI and useful comments on emission inventories. The authors are also thankful for Ms. Natsumi Tanji of JMA and Mr. Yuma Imai and Yusuke Otsu of University of Tsukuba for data processing. The authors are also thankful for Drs. Masayoshi Ishii, Akinori Takami, Seiji Sugata, and Tatsuya Nagashima of University of Tsukuba, Corporative Graduate School Program and Dr. Akio Yamagami of MRI, Dr. Joseph Ching of University of Tottori, Mr. Tomoki Kajikawa, Ms. Rio Ishikawa, and Mr. Takuya Nakagawa of University of Tsukuba for useful discussion and comments on this study. This research was supported by Japanese Society for the Promotion of Sciences (JSPS) Grant-in-Aid for JSPS Fellows Grant Nos. JP21J22912 and Environmental Research and Technology Development Fund of the Environmental Restoration and Conservation Agency (ERCA) (JPMEERF20215003).

Conflict of interest

The authors declare no conflicts of interest relevant to this study.

Data availability statement

The NHM-Chem source code is available at subject to a license agreement with the Meteorological Research Institute. Further information is available at https://www.mri-jma.go.jp/Dep/glb/nhmchem_model/application_en.html (last accessed: 23 January 2023). The raw data of REASv3.2.1 provided by Kurokawa and Ohara (2020) used for the anthropogenic emission inventory in Northeast Asia can be obtained from https://www.nies.go.jp/REAS/ (last accessed: 23 January 2023). The raw data of GFED v4 used for the biomass burning emission inventory provided by Giglio et al. (2013) can be obtained from https://www.globalfiredata.org/data.html (last accessed: 23 January 2023). The metal emission inventory data of TMI-Asia v1.1 developed in this study is available from Kayaba (2023) (https://doi.org/10.17632/r9c59639pg.1). The data of TMI-Japan v1.1 cannot be uploaded due to excess cloud capacity, so please contact the author if you need that. The metal content rates in $PM_{2.5}$ or PM_{10} used in the TMI-Asia/Japan v1.1 development are indicated in the Supporting excel file. The observation data of MOE $PM_{2.5}$ survey are available at https://www.env.go.jp/air/osen/pm/monitoring.html (last accessed: 23 January 2023). The map figures in this paper were drawn with GrADS v2.0. The GrADS software provided by Center for Ocean-Land-Atmosphere Studies (COLA) van be obtained at http://cola.gmu.edu/grads/ (last accessed: December 14, 2022).

References

Alam, Md. S., Hyde, B., Duffy, P., & McNabola, A. (2018). Analysing the Co-Benefits of transport fleet and fuel policies in reducing $PM_{2.5}$ and CO_2 emissions. *Journal of Cleaner Production*, *172*, 623–634. https://doi.org/10.1016/j.jclepro.2017.10.169

Alves, C. A., Evtyugina, M., Vicente, A. M. P., Vicente, E. D., Nunes, T. V., Silva, P. M. A., Duarte, M. A. C., Pio, C. A., Amato, F., & Querol, X. (2018). Chemical profiling of PM_{10} from urban road dust. *Science of The Total Environment*, *634*, 41–51. https://doi.org/10.1016/j.scitotenv.2018.03.338

Barlow, T. (2014). *Briefing paper on non-exhaust particulate emissions from road transport.* Wokingham, UK: Transport Research Laboratory.

Bates, J. T., Fang, T., Verma, V., Zeng, L., Weber, R. J., Tolbert, P. E., Abrams, J. Y., Sarnat, S. E., Klein, M., Mulholland, J. A., & Russell, A. G. (2019). Review of Acellular Assays of Ambient Particulate Matter Oxidative Potential: Methods and Relationships with Composition, Sources, and Health Effects. *Environmental Science & Technology*, *53*(8), 4003–4019. https://doi.org/10.1021/acs.est.8b03430

Beddows, D. C. S., & Harrison, R. M. (2021). PM_{10} and $PM_{2.5}$ emission factors for non-exhaust particles from road vehicles: Dependence upon vehicle mass and implications for battery electric vehicles. *Atmospheric Environment*, *244*, 117886. https://doi.org/10.1016/j.atmosenv.2020.117886

Blok, J. (2005). Environmental exposure of road borders to zinc. *Science of The Total Environment*, *348*(1–3), 173–190. https://doi.org/10.1016/j.scitotenv.2004.12.073

Cadle, S. H., Mulawa, P. A., Ball, J., Donase, C., Weibel, A., Sagebiel, J. C., Knapp, K. T., & Snow, R. (1997). Particulate Emission Rates from In-Use High-Emitting Vehicles Recruited in Orange County, California. *Environmental Science & Technology*, *31*(12), 3405–3412. https://doi.org/10.1021/es9700257

Central Environment Council, Ministry of Environment. (2003). *Future Measures to Reduce Vehicle Emissions (Seventh Report)*. https://www.env.go.jp/council/toshin/t07-h1502/t07-h1502_1.pdf

Central Environment Council, Ministry of Environment. (2022). *Future Measures to Reduce Vehicle Emissions (Fourteenth Report)*. https://www.env.go.jp/content/900400276.pdf

Center for Ocean-Land-Atmosphere Studies. (2023). Grid Analysis and Display System (GrADS) version 2.0 [Software]. http://cola.gmu.edu/grads/grads.php (last accessed: 23 January 2023)

Charrier, J. G., & Anastasio, C. (2011). Impacts of antioxidants on hydroxyl radical production from individual and mixed transition metals in a surrogate lung fluid. *Atmospheric Environment*, *45*(40), 7555–7562. https://doi.org/10.1016/j.atmosenv.2010.12.021

Charrier, J. G., & Anastasio, C. (2012). On dithiothreitol (DTT) as a measure of oxidative potential for ambient particles: evidence for the importance of soluble transition metals. *Atmospheric Chemistry and Physics*, *12*(19), 9321–9333. https://doi.org/10.5194/acp-12-9321-2012

Chen, H., & Grassian, V. H. (2013). Iron Dissolution of Dust Source Materials during Simulated Acidic Processing: The Effect of Sulfuric, Acetic, and Oxalic Acids. *Environmental Science & Technology*, *47*(18), 10312–10321. https://doi.org/10.1021/es401285s

Chow, J. C., Watson, J. G., Kuhns, H., Etyemezian, V., Lowenthal, D. H., Crow, D., Kohl, S. D., Engelbrecht, J. P., & Green, M. C. (2004). Source profiles for industrial, mobile, and area sources in the Big Bend

Regional Aerosol Visibility and Observational study. *Chemosphere*, *54*(2), 185–208. https://doi.org/10.1016/j.chemosphere.2003.07.004

Clarke, A. D., Owens, S. R., & Zhou, J. (2006). An ultrafine sea-salt flux from breaking waves: Implications for cloud condensation nuclei in the remote marine atmosphere. *Journal of Geophysical Research: Atmosphere*, *111*(D6), D06202. https://doi.org/10.1029/2005JD006565

Clegg, S. L., Brimblecombe, P., & Wexler, A. S. (1998). Thermodynamic Model of the System H^+–NH_4+–SO_4^{2-}–NO_3^-–H_2O at Tropospheric Temperatures. *The Journal of Physical Chemistry A*, *102*(12), 2137–2154. https://doi.org/10.1021/jp973042r

Clegg, S. L., & Brimblecombe, Peter. (1990). Equilibrium partial pressures and mean activity and osmotic coefficients of 0-100% nitric acid as a function of temperature. *The Journal of Physical Chemistry*, *94*(13), 5369–5380. https://doi.org/10.1021/j100376a038

Denier van der Gon, H. A. C., Gerlofs-Nijland, M. E., Gehrig, R., Gustafsson, M., Janssen, N., Harrison, R. M., Hulskotte, J., Johansson, C., Jozwicka, M., Keuken, M., Krijgsheld, K., Ntziachristos, L., Riediker, M., & Cassee, F. R. (2013). The Policy Relevance of Wear Emissions from Road Transport, Now and in the Future—An International Workshop Report and Consensus Statement. *Journal of the Air & Waste Management Association*, *63*(2), 136–149. https://doi.org/10.1080/10962247.2012.741055

Desboeufs, K. V., Sofikitis, A., Losno, R., Colin, J. L., & Ausset, P. (2005). Dissolution and solubility of trace metals from natural and anthropogenic aerosol particulate matter. *Chemosphere*, *58*(2), 195–203. https://doi.org/10.1016/j.chemosphere.2004.02.025

Deushi, M., & Shibata, K. (2011). Development of a Meteorological Research Institute Chemistry-Climate Model version 2 for the Study of Tropospheric and Stratospheric Chemistry. *Papers in Meteorology and Geophysics*, *62*, 1–46. https://doi.org/10.2467/mripapers.62.1

Ding, J., Zhao, P., Su, J., Dong, Q., Du, X., & Zhang, Y. (2019). Aerosol pH and its driving factors in Beijing. *Atmospheric Chemistry and Physics*, *19*(12), 7939–7954. https://doi.org/10.5194/acp-19-7939-2019

European Environment Agency. (2011). *Air pollution impacts from carbon capture and storage (CCS)*. Retrieved from https://doi.org/doi:10.2800/84208

European Monitoring and Evaluation Programme / European Environment Agency. (2019). *EMEP/EEA air pollutant emission inventory guidebook 2019 : Technical guidance to prepare national emission inventories*. Publications Office of the European Union. Retrieved from https://www.eea.europa.eu/publications/emep-eea-guidebook-2019

Fang, T., Guo, H., Zeng, L., Verma, V., Nenes, A., & Weber, R. J. (2017). Highly Acidic Ambient Particles, Soluble Metals, and Oxidative Potential: A Link between Sulfate and Aerosol Toxicity. *Environmental Science & Technology*, *51*(5), 2611–2620. https://doi.org/10.1021/acs.est.6b06151

Fountoukis, C., & Nenes, A. (2007). ISORROPIA II: a computationally efficient thermodynamic equilibrium model for K^+-Ca^{2+}-Mg^{2+}-NH^{4+}-Na^+-SO_4^{2-}-NO_3^--Cl^--H_2O aerosols. *Atmospheric Chemistry and Physics*, *7*, 4639–4659. http://www.atmos-chem-phys.net/7/4639/2007/

Fountoukis, C., Nenes, A., Sullivan, A., Weber, R., van Reken, T., Fischer, M., Matías, E., Moya, M., Farmer, D., & Cohen, R. C. (2009). Thermodynamic characterization of Mexico City aerosol during MILAGRO 2006. *Atmospheric Chemistry and Physics*, *9*, 2141–2156. https://doi.org/10.5194/acp-9-2141-2009

Fukui, T., Kokuryo, K., Baba, T., & Kannari, A. (2014). Updating EAGrid2000-Japan emissions inventory based on the recent emission trends. *Journal of Japan Society for Atmospheric Environment*, *49*(2), 117–125. https://doi.org/10.11298/taiki.49.117 (in Japanese)

Fussell, J. C., Franklin, M., Green, D. C., Gustafsson, M., Harrison, R. M., Hicks, W., Kelly, F. J., Kishta, F., Miller, M. R., Mudway, I. S., Oroumiyeh, F., Selley, L., Wang, M., & Zhu, Y. (2022). A Review of Road Traffic-Derived Non-Exhaust Particles: Emissions, Physicochemical Characteristics, Health Risks, and Mitigation Measures. *Environmental Science & Technology*, *56*(11), 6813–6835. https://doi.org/10.1021/acs.est.2c01072

Gant, T. W., Ramakrishna Rao, D. N., Mason, R. P., & Cohen, G. M. (1988). Redox cycling and sulphydryl arylation; Their relative importance in the mechanism of quinone cytotoxicity to isolated hepatocytes. *Chemico-Biological Interactions*, *65*(2), 157–173. https://doi.org/10.1016/0009-2797(88)90052-X

Garg, B. D., Cadle, S. H., Mulawa, P. A., Groblicki, P. J., Laroo, C., & Parr, G. A. (2000). Brake Wear Particulate Matter Emissions. *Environmental Science & Technology*, *34*(21), 4463–4469. https://doi.org/10.1021/es001108h

Giglio, L., Randerson, J. T., & van der Werf, G. R. (2013). Analysis of daily, monthly, and annual burned area using the fourth-generation global fire emissions database (GFED4). *Journal of Geophysical Research: Biogeosciences*, *118*(1), 317–328. https://doi.org/10.1002/jgrg.20042

Giglio, L., Randerson, J.T. and Van Der Werf, G.R. (2013). Global Fire Emissions Database version 4 [Dataset]. https://www.globalfiredata.org/ (last accessed: 23 January 2023)

Gottipolu, R. R., Landa, E. R., Schladweiler, M. C., McGee, J. K., Ledbetter, A. D., Richards, J. H., Wallenborn, G. J., & Kodavanti, U. P. (2008). Cardiopulmonary Responses of Intratracheally Instilled Tire Particles and Constituent Metal Components. *Inhalation Toxicology*, *20*(5), 473–484. https://doi.org/10.1080/08958370701858427

Grigoratos, Theodoros., & Martini, Giorgio. (2014). *Non-exhaust traffic related emissions - Brake and tyre wear PM literature review.* Ispra, Italy: Joint Research Centre. Retrieved from https://publications.jrc.ec.europa.eu/repository/handle/JRC89231

Guenther, A., Karl, T., Harley, P., Wiedinmyer, C., Palmer, P. I., & Geron, C. (2006). Estimates of global terrestrial isoprene emissions using MEGAN (Model of Emissions of Gases and Aerosols from Nature). *Atmospheric Chemistry and Physics*, *6*, 3181–3210. https://doi.org/10.5194/acp-6-3181-2006

Guo, H., Liu, J., Froyd, K. D., Roberts, J. M., Veres, P. R., Hayes, P. L., Jimenez, J. L., Nenes, A., & Weber, R. J. (2017). Fine particle pH and gas–particle phase partitioning of inorganic species in Pasadena, California, during the 2010 CalNex campaign. *Atmospheric Chemistry and Physics*, *17*(9), 5703–5719. https://doi.org/10.5194/acp-17-5703-2017

Guo, H., Otjes, R., Schlag, P., Kiendler-Scharr, A., Nenes, A., & Weber, R. J. (2018). Effectiveness of ammonia reduction on control of fine particle nitrate. *Atmospheric Chemistry and Physics*, *18*(16), 12241–12256. https://doi.org/10.5194/acp-18-12241-2018

Guo, H., Sullivan, A. P., Campuzano-Jost, P., Schroder, J. C., Lopez-Hilfiker, F. D., Dibb, J. E., Jimenez, J. L., Thornton, J. A., Brown, S. S., Nenes, A., & Weber, R. J. (2016). Fine particle pH and the partitioning of nitric acid during winter in the northeastern United States. *Journal of Geophysical Research: Atmospheres*, *121*(17), 10355–10376. https://doi.org/10.1002/2016JD025311

Guo, H., Xu, L., Bougiatioti, A., Cerully, K. M., Capps, S. L., Hite, J. R., Carlton, A. G., Lee, S.-H., Bergin, M. H., Ng, N. L., Nenes, A., & Weber, R. J. (2015). Fine-particle water and pH in the southeastern United States. *Atmospheric Chemistry and Physics*, *15*(9), 5211–5228. https://doi.org/10.5194/acp-15-5211-2015

Gutteridge, J. M. C. (1995). Lipid peroxidation and antioxidants as biomarkers of tissue damage. *Clinical Chemistry*, *41*(12), 1819–1828. https://doi.org/10.1093/clinchem/41.12.1819

Hall, T. (2017). A Comparison of Braking Behavior between an IC Engine and Pure Electric Vehicle in Los Angeles City Driving Conditions. SAE Technical Paper 2017-01-2518. https://doi.org/10.4271/2017-01-2518.

Hagino, H. (2019). Sensitivity and Reproducibility of Brake Wear Particle Emission Measurements using JARI System. In *50th PMP Meeting*. Retrieved from https://wiki.unece.org/download/attachments/75532498/2019-04-02_09-JARI%20Brake%20Emission.pdf?api=v2 (last accessed: 22 January 2023)

Hagino, H. (2020). Brake Wear Particle Emissions from Automotive. *Journal of Japan Society for Atmospheric Environment*, *55*(2), A18–A35. https://doi.org/10.11298/taiki.55.A18 (in Japanese)

Hagino, H., Oyama, M., & Sasaki, S. (2016). Laboratory testing of airborne brake wear particle emissions using a dynamometer system under urban city driving cycles. *Atmospheric Environment*, *131*, 269–278. https://doi.org/10.1016/j.atmosenv.2016.02.014

Han, Z., Ueda, H., Matsuda, K., Zhang, R., Arao, K., Kanai, Y., & Hasome, H. (2004). Model study on particle size segregation and deposition during Asian dust events in March 2002. *Journal of Geophysical Research: Atmospheres*, *109*(D19), D19205. https://doi.org/10.1029/2004JD004920

Hao, H., Wang, H., Ouyang, M., & Cheng, F. (2011). Vehicle survival patterns in China. *Science China Technological Sciences*, *54*(3), 625–629. https://doi.org/10.1007/s11431-010-4256-1

Harrison, R. M., Allan, J., Carruthers, D., Heal, M. R., Lewis, A. C., Marner, B., Murrells, T., & Williams, A. (2021). Non-exhaust vehicle emissions of particulate matter and VOC from road traffic: A review. *Atmospheric Environment*, *262*, 118592. https://doi.org/10.1016/j.atmosenv.2021.118592

Hildemann, L. M., Markowski, G. R., & Cass, G. R. (1991). Chemical composition of emissions from urban sources of fine organic aerosol. *Environmental Science & Technology*, *25*(4), 744–759. https://doi.org/10.1021/es00016a021

Hooftman, N., Oliveira, L., Messagie, M., Coosemans, T., & van Mierlo, J. (2016). Environmental Analysis of Petrol, Diesel and Electric Passenger Cars in a Belgian Urban Setting. *Energies*, *9*(2), 84. https://doi.org/10.3390/en9020084

Hori, M., & Kaneda, T. (2012). Fuel Consumption Metrics of PHEV by the Equivalent Composite of Electricity and Gasoline. *Transactions of Society of Automotive Engineers of Japan*, *43*(6), 1401–1405. https://doi.org/10.11351/jsaeronbun.43.1401 (in Japanese)

Huo, H., & Wang, M. (2012). Modeling future vehicle sales and stock in China. *Energy Policy*, *43*, 17–29. https://doi.org/10.1016/j.enpol.2011.09.063

Iijima, A., Sato, K., Yano, K., Kato, M., Kozawa, K., & Furuta, N. (2008). Emission Factor for Antimony in Brake Abrasion Dusts as One of the Major Atmospheric Antimony Sources. *Environmental Science & Technology*, *42*(8), 2937–2942. https://doi.org/10.1021/es702137g

International Energy Agency. (2021). *Japan 2021 - Energy Policy Review*. Retrieved from https://iea.blob.core.windows.net/assets/3470b395-cfdd-44a9-9184-0537cf069c3d/Japan2021_EnergyPolicyReview.pdf

Islam, E., Moawad, A., Kim, N., & Rousseau, A. (2020). *Energy Consumption and Cost Reduction of Future Light-Duty Vehicles through Advanced Vehicle Technologies: A Modeling Simulation Study Through 2050*. Illinois: Argonne National Laboratory. Retrieved from https://doi.org/10.2172/1647165

Ito, A. (2015). Atmospheric Processing of Combustion Aerosols as a Source of Bioavailable Iron. *Environmental Science & Technology Letters*, *2*(3), 70–75. https://doi.org/10.1021/acs.estlett.5b00007

Ito, A., Ye, Y., Baldo, C., & Shi, Z. (2021). Ocean fertilization by pyrogenic aerosol iron. *Npj Climate and Atmospheric Science*, *4*(1), 30. https://doi.org/10.1038/s41612-021-00185-8

Jiang, Ahmed, Canchola, Chen, & Lin. (2019). Use of Dithiothreitol Assay to Evaluate the Oxidative Potential of Atmospheric Aerosols. *Atmosphere*, *10*(10), 571. https://doi.org/10.3390/atmos10100571

Kajino, M., Deushi, M., Sekiyama, T. T., Oshima, N., Yumimoto, K., Tanaka, T. Y., Ching, J., Hashimoto, A., Yamamoto, T., Ikegami, M., Kamada, A., Miyashita, M., Inomata, Y., Shima, S., Khatri, P., Shimizu, A., Irie, H., Adachi, K., Zaizen, Y., … Mikami, M. (2021). Comparison of three aerosol representations of NHM-Chem (v1.0) for the simulations of air quality and climate-relevant variables. *Geoscientific Model Development*, *14*(4), 2235–2264. https://doi.org/10.5194/gmd-14-2235-2021

Kajino, M., Deushi, M., Sekiyama, T. T., Oshima, N., Yumimoto, K., Tanaka, T. Y., Ching, J., Hashimoto, A., Yamamoto, T., Ikegami, M., Kamada, A., Miyashita, M., Inomata, Y., Shima, S., Takami, A., Shimizu, A., Hatakeyama, S., Sadanaga, Y., Irie, H., … Mikami, M. (2019a). NHM-Chem, the Japan Meteorological Agency's Regional Meteorology – Chemistry Model: Model Evaluations toward the Consistent Predictions of the Chemical, Physical, and Optical Properties of Aerosols. *Journal of the Meteorological Society of Japan. Ser. II*, *97*(2), 337–374. https://doi.org/10.2151/jmsj.2019-020

Kajino, M., Hagino, H., Fujitani, Y., Morikawa, T., Fukui, T., Onishi, K., Okuda, T., Kajikawa, T., & Igarashi, Y. (2020). Modeling Transition Metals in East Asia and Japan and Its Emission Sources. *GeoHealth*, *4*(9). https://doi.org/10.1029/2020GH000259

Kajino, M., Sekiyama, T. T., Igarashi, Y., Katata, G., Sawada, M., Adachi, K., Zaizen, Y., Tsuruta, H., & Nakajima, T. (2019b). Deposition and Dispersion of Radio-Cesium Released Due to the Fukushima Nuclear Accident: Sensitivity to Meteorological Models and Physical Modules. *Journal of Geophysical Research: Atmospheres*, *124*(3), 1823–1845. https://doi.org/10.1029/2018JD028998

Kannari, A., Tonooka, Y., Baba, T., & Murano, K. (2007). Development of multiple-species 1km×1km resolution hourly basis emissions inventory for Japan. *Atmospheric Environment*, *41*(16), 3428–3439. https://doi.org/10.1016/j.atmosenv.2006.12.015

Katritzky, A., Fedoseyenko, D., Mohapatra, P., & Steel, P. (2008). Reactions of p-Benzoquinone with Sulfur Nucleophiles. *Synthesis*, *2008*(5), 777–787. https://doi.org/10.1055/s-2008-1032186

Kayaba, S., Kajino, M. (2022). Impact of battery electric vehicle penetration and corresponding changes in upstream processes on summer O_3 concentrations in Japan. ESSOAr. https://doi.org/10.1002/essoar.10512177.1

Kayaba, S. (2023). TMI-Asia v1.1, Mendeley Data, V1 [Dataset]. https://doi.org/10.17632/r9c59639pg.1

Ke, W., Zhang, S., Wu, Y., Zhao, B., Wang, S., & Hao, J. (2017). Assessing the Future Vehicle Fleet Electrification: The Impacts on Regional and Urban Air Quality. *Environmental Science & Technology*, *51*(2), 1007–1016. https://doi.org/10.1021/acs.est.6b04253

Kelly, J. C., Sullivan, J. L., Burnham, A., & Elgowainy, A. (2015). Impacts of Vehicle Weight Reduction via Material Substitution on Life-Cycle Greenhouse Gas Emissions. *Environmental Science & Technology*, *49*(20), 12535–12542. https://doi.org/10.1021/acs.est.5b03192

Kendrick, E., & Kulkarni, P. (2019). *Quantifying the Environmental Impacts of Braking Emissions*. https://core.ac.uk/download/pdf/224975744.pdf

Kitamori, Y., Mochida, M., & Kawamura, K. (2009). Assessment of the aerosol water content in urban atmospheric particles by the hygroscopic growth measurements in Sapporo, Japan. *Atmospheric Environment*, *43*(21), 3416–3423. https://doi.org/10.1016/j.atmosenv.2009.03.037

Klimont, Z., Kupiainen, K., Heyes, C., Purohit, P., Cofala, J., Rafaj, P., Borken-Kleefeld, J., & Schöpp, W. (2017). Global anthropogenic emissions of particulate matter including black carbon. *Atmospheric Chemistry and Physics*, *17*(14), 8681–8723. https://doi.org/10.5194/acp-17-8681-2017

Kobayashi, S., Ota, Y., Harada, Y., Ebita, A., Moriya, M., Onoda, H., Onogi, K., Kamahori, H., Kobayashi, C., Endo, H., Miyaoka, K., & Takahashi, K. (2015). The JRA-55 Reanalysis: General Specifications and Basic Characteristics. *Journal of the Meteorological Society of Japan. Ser. II*, *93*(1), 5–48. https://doi.org/10.2151/jmsj.2015-001

Kumagai, Y., Koide, S., Taguchi, K., Endo, A., Nakai, Y., Yoshikawa, T., & Shimojo, N. (2002). Oxidation of Proximal Protein Sulfhydryls by Phenanthraquinone, a Component of Diesel Exhaust Particles. *Chemical Research in Toxicology*, *15*(4), 483–489. https://doi.org/10.1021/tx0100993

Kumagai, Y., Shinkai, Y., Miura, T., & Cho, A. K. (2012). The Chemical Biology of Naphthoquinones and Its Environmental Implications. *Annual Review of Pharmacology and Toxicology*, *52*(1), 221–247. https://doi.org/10.1146/annurev-pharmtox-010611-134517

Kurokawa, J. and Ohara, T. (2020). Regional Emission inventory in ASia (REAS) version 3.2.1 [Dataset]. https://www.nies.go.jp/REAS/ (last accessed: 23 January 2023)

Kurokawa, J., & Ohara, T. (2020). Long-term historical trends in air pollutant emissions in Asia: Regional Emission inventory in ASia (REAS) version 3. *Atmospheric Chemistry and Physics*, *20*(21), 12761–12793. https://doi.org/10.5194/acp-20-12761-2020

Kurokawa, J., Ohara, T., Morikawa, T., Hanayama, S., Janssens-Maenhout, G., Fukui, T., Kawashima, K., & Akimoto, H. (2013). Emissions of air pollutants and greenhouse gases over Asian regions during 2000–2008: Regional Emission inventory in ASia (REAS) version 2. *Atmospheric Chemistry and Physics*, *13*(21), 11019–11058. https://doi.org/10.5194/acp-13-11019-2013

Lakey, P. S. J., Berkemeier, T., Tong, H., Arangio, A. M., Lucas, K., Pöschl, U., & Shiraiwa, M. (2016). Chemical exposure-response relationship between air pollutants and reactive oxygen species in the human respiratory tract. *Scientific Reports*, *6*(1), 32916. https://doi.org/10.1038/srep32916

Lawal, A. S., Guan, X., Liu, C., Henneman, L. R. F., Vasilakos, P., Bhogineni, V., Weber, R. J., Nenes, A., & Russell, A. G. (2018). Linked Response of Aerosol Acidity and Ammonia to SO_2 and NO_x Emissions Reductions in the United States. *Environmental Science & Technology*, *52*(17), 9861–9873. https://doi.org/10.1021/acs.est.8b00711

Li, N., Chen, J.-P., Tsai, I.-C., He, Q., Chi, S.-Y., Lin, Y.-C., & Fu, T.-M. (2016). Potential impacts of electric vehicles on air quality in Taiwan. *Science of The Total Environment*, *566–567*, 919–928. https://doi.org/10.1016/j.scitotenv.2016.05.105

Lin, M., & Yu, J. Z. (2020). Assessment of Interactions between Transition Metals and Atmospheric Organics: Ascorbic Acid Depletion and Hydroxyl Radical Formation in Organic-Metal Mixtures. *Environmental Science & Technology*, *54*(3), 1431–1442. https://doi.org/10.1021/acs.est.9b07478

Lough, G. C., Schauer, J. J., Park, J.-S., Shafer, M. M., DeMinter, J. T., & Weinstein, J. P. (2005). Emissions of Metals Associated with Motor Vehicle Roadways. *Environmental Science & Technology*, *39*(3), 826–836. https://doi.org/10.1021/es048715f

Lu, Z., Zhou, Y., Cai, H., Wang, M., He, X., & Przesmitzki, S. (2018). *China Vehicle Fleet Model: Estimation of Vehicle Stocks, Usage, Emissions, and Energy Use - Model Description, Technical Documentation, and User Guide*. Illinois: Argonne National Laboratory. Retrieved from https://publications.anl.gov/anlpubs/2018/11/148761.pdf

McWhinney, R. D., Zhou, S., & Abbatt, J. P. D. (2013). Naphthalene SOA: redox activity and naphthoquinone gas–particle partitioning. *Atmospheric Chemistry and Physics*, *13*(19), 9731–9744. https://doi.org/10.5194/acp-13-9731-2013

Mehlig, D., Woodward, H., Oxley, T., Holland, M., & ApSimon, H. (2021). Electrification of Road Transport and the Impacts on Air Quality and Health in the UK. *Atmosphere*, *12*(11), 1491. https://doi.org/10.3390/atmos12111491

Meskhidze, N., Chameides, W. L., Nenes, A., & Chen, G. (2003). Iron mobilization in mineral dust: Can anthropogenic SO_2 emissions affect ocean productivity? *Geophysical Research Letters*, *30*(21), 2085. https://doi.org/10.1029/2003GL018035

Meteorological Research Institute. (2022). Application for use of Japan Meteorological Agency's regional-scale meteorology-chemistry model [Software]. https://www.mri-jma.go.jp/Dep/glb/nhmchem_model/application_en.html (last accessed: 23 January 2023)

Miller, W. P., Zelazny, L. W., & Martens, D. C. (1986). Dissolution of synthetic crystalline and noncrystalline iron oxides by organic acids. *Geoderma*, *37*(1), 1–13. https://doi.org/10.1016/0016-7061(86)90039-X

Ministry of Economy. (2023). Results of mass concentration and component measurement of fine particulate matter ($PM_{2.5}$) [Dataset]. https://www.env.go.jp/air/osen/pm/monitoring.html (last accessed: 23 January 2023)

Ministry of Economy, Trade and Industry. (2019). Energy White Paper 2019 – HTML version. https://www.enecho.meti.go.jp/about/whitepaper/2019html/2-1-4.html (last accessed: 20 January 2023) (in Japanese)

Ministry of Economy, Trade and Industry. (2021). Strategies to achieve carbon neutrality in 2050. https://www.enecho.meti.go.jp/committee/council/basic_policy_subcommittee/2021/043/043_004.pdf (last accessed: 20 January 2023) (in Japanese)

Ministry of Land, Infrastructure and Transport. (2010). National Road and Street Traffic Conditions Survey (Road Traffic Census). https://www.mlit.go.jp/road/census/h22-1/data/pdf/syuukei04.pdf (last accessed: 20 January 2023) (in Japanese)

Ministry of Land, Infrastructure and Transport. (2012). Annual Report on Fuel Consumption of Automobiles for FY2012. https://www.mlit.go.jp/k-

toukei/22/errata/kaitei/annual/pdf/new/22201200a00000_n.pdf (last accessed: 22 January 2023) (in Japanese)

Ministry of Land, Infrastructure and Transport, urban bureau, (2012), Guidelines for the Installation of Charging Facilities in Parking Lots, etc. Guidelines for the Installation of Charging Facilities in Parking Lots, etc., https://www.mlit.go.jp/common/000212869.pdf (last accessed: 22 January 2023) (in Japanese)

Moawad, A., Kim, N., Shidore, N., & Rousseau, A. (2016). *Assessment of Vehicle Sizing, Energy Consumption, and Cost through Large-Scale Simulation of Advanced Vehicle Technologies*. Illinois: Argonne National Laboratory. Retrieved from https://doi.org/10.2172/1250463

Moawad, A., Sharer, P., & Rousseau, A. (2011). *Light-Duty Vehicle Fuel Consumption Displacement Potential up to 2045*. Illinois: Argonne National Laboratory. Retrieved from https://doi.org/10.2172/1250463

Morikawa, T. (2017). Current Status of Japanese Emission Inventory for PM 2.5 and its Problems. *Journal of Japan Society for Atmospheric Environment*, *52*(3). https://doi.org/10.11298/taiki.52.A74 (in Japanese)

Muramoto, K., Hirata, K., Shinzawa-Itoh, K., Yoko-o, S., Yamashita, E., Aoyama, H., Tsukihara, T., & Yoshikawa, S. (2007). A histidine residue acting as a controlling site for dioxygen reduction and proton pumping by cytochrome c oxidase. *Proceedings of the National Academy of Sciences*, *104*(19), 7881–7886. https://doi.org/10.1073/pnas.0610031104

Nenes, A., Pandis, S. N., Weber, R. J., & Russell, A. (2020). Aerosol pH and liquid water content determine when particulate matter is sensitive to ammonia and nitrate availability. *Atmospheric Chemistry and Physics*, *20*(5), 3249–3258. https://doi.org/10.5194/acp-20-3249-2020

Nishikawa, M., Batdorj, D., Ukachi, M., Onishi, K., Nagano, K., Mori, I., Matsui, I. and Sano, T. (2013). Preparation and chemical characterisation of an Asian mineral dust certified reference material. *Analytical Methods*, 5 (16), 4088–4095. https://doi.org/10.1039/C3AY40435H

Nopmongcol, U., Grant, J., Knipping, E., Alexander, M., Schurhoff, R., Young, D., Jung, J., Shah, T., & Yarwood, G. (2017). Air Quality Impacts of Electrifying Vehicles and Equipment Across the United States. *Environmental Science & Technology*, *51*(5), 2830–2837. https://doi.org/10.1021/acs.est.6b04868

Oakes, M., Ingall, E. D., Lai, B., Shafer, M. M., Hays, M. D., Liu, Z. G., Russell, A. G., & Weber, R. J. (2012). Iron Solubility Related to Particle Sulfur Content in Source Emission and Ambient Fine Particles. *Environmental Science & Technology*, *46*(12), 6637–6644. https://doi.org/10.1021/es300701c

Organisation for Economic Cooperation and Development. (2020). *Non-exhaust Particulate Emissions from Road Transport*. https://www.actu-environnement.com/media/pdf/news-36643-rapport-ocde-emissions-hors-echappement.pdf

Paglione, M., Decesari, S., Rinaldi, M., Tarozzi, L., Manarini, F., Gilardoni, S., Facchini, M. C., Fuzzi, S., Bacco, D., Trentini, A., Pandis, S. N., & Nenes, A. (2021). Historical Changes in Seasonal Aerosol Acidity in the Po Valley (Italy) as Inferred from Fog Water and Aerosol Measurements. *Environmental Science & Technology*, *55*(11), 7307–7315. https://doi.org/10.1021/acs.est.1c00651

Pan, S., Roy, A., Choi, Y., Eslami, E., Thomas, S., Jiang, X., & Gao, H. O. (2019). Potential impacts of electric vehicles on air quality and health endpoints in the Greater Houston Area in 2040. *Atmospheric Environment*, *207*, 38–51. https://doi.org/10.1016/j.atmosenv.2019.03.022

Paris, R., & Desboeufs, K. v. (2013). Effect of atmospheric organic complexation on iron-bearing dust solubility. *Atmospheric Chemistry and Physics*, *13*(9), 4895–4905. https://doi.org/10.5194/acp-13-4895-2013

Platform for Electro-mobility. (2016). *Briefing: Non-Exhaust Emissions of Electric Cars*. http://www.platformelectromobility.eu/wp-content/uploads/2016/06/Briefing_Electro-Mobility-Platform-responds-to-studies-on-tyre-emissions-from-EVs.pdf

Pope, C. A., & Dockery, D. W. (2006). Health Effects of Fine Particulate Air Pollution: Lines that Connect. *Journal of the Air & Waste Management Association*, *56*(6), 709–742. https://doi.org/10.1080/10473289.2006.10464485

Pye, H. O. T., Zuend, A., Fry, J. L., Isaacman-VanWertz, G., Capps, S. L., Appel, K. W., Foroutan, H., Xu, L., Ng, N. L., & Goldstein, A. H. (2018). Coupling of organic and inorganic aerosol systems and the effect on gas–particle partitioning in the southeastern US. *Atmospheric Chemistry and Physics*, *18*(1), 357–370. https://doi.org/10.5194/acp-18-357-2018

Qin, L., Mills, D. A., Hiser, C., Murphree, A., Garavito, R. M., Ferguson-Miller, S., & Hosler, J. (2007). Crystallographic Location and Mutational Analysis of Zn and Cd Inhibitory Sites and Role of Lipidic Carboxylates in Rescuing Proton Path Mutants in Cytochrome c Oxidase. *Biochemistry*, *46*(21), 6239–6248. https://doi.org/10.1021/bi700173w

Samet, J. M., Chen, H., Pennington, E. R., & Bromberg, P. A. (2020). Non-redox cycling mechanisms of oxidative stress induced by PM metals. *Free Radical Biology and Medicine*, *151*, 26–37. https://doi.org/10.1016/j.freeradbiomed.2019.12.027

Samet, J. M., Graves, L. M., Quay, J., Dailey, L. A., Devlin, R. B., Ghio, A. J., Wu, W., Bromberg, P. A., & Reed, W. (1998). Activation of MAPKs in human bronchial epithelial cells exposed to metals. *American Journal of Physiology-Lung Cellular and Molecular Physiology*, *275*(3), L551–L558. https://doi.org/10.1152/ajplung.1998.275.3.L551

Samet, J. M., Silbajoris, R., Wu, W., & Graves, L. M. (1999). Tyrosine Phosphatases as Targets in Metal-Induced Signaling in Human Airway Epithelial Cells. *American Journal of Respiratory Cell and Molecular Biology*, *21*(3), 357–364. https://doi.org/10.1165/ajrcmb.21.3.3656

Sanders, P. G., Xu, N., Dalka, T. M., & Maricq, M. M. (2003). Airborne Brake Wear Debris: Size Distributions, Composition, and a Comparison of Dynamometer and Vehicle Tests. *Environmental Science & Technology*, *37*(18), 4060–4069. https://doi.org/10.1021/es034145s

Sato, F. E. K., & Nakata, T. (2019). Recoverability Analysis of Critical Materials from Electric Vehicle Lithium-Ion Batteries through a Dynamic Fleet-Based Approach for Japan. *Sustainability*, *12*(1), 147. https://doi.org/10.3390/su12010147

Schnell, J. L., Naik, V., Horowitz, L. W., Paulot, F., Ginoux, P., Zhao, M., & Horton, D. E. (2019). Air quality impacts from the electrification of light-duty passenger vehicles in the United States. *Atmospheric Environment*, *208*, 95–102. https://doi.org/10.1016/j.atmosenv.2019.04.003

Schroth, A. W., Crusius, J., Sholkovitz, E. R., & Bostick, B. C. (2009). Iron solubility driven by speciation in dust sources to the ocean. *Nature Geoscience*, *2*(5), 337–340. https://doi.org/10.1038/ngeo501

Seinfeld, J. H. and Pandis, S. N. (2016). Atmospheric Chemistry and Physics: From Air Pollution to Climate Change Third Edition.

Shahpoury, P., Zhang, Z. W., Arangio, A., Celo, V., Dabek-Zlotorzynska, E., Harner, T., & Nenes, A. (2021). The influence of chemical composition, aerosol acidity, and metal dissolution on the oxidative potential of fine particulate matter and redox potential of the lung lining fluid. *Environment International*, *148*, 106343. https://doi.org/10.1016/j.envint.2020.106343

Shiraiwa, M., Ueda, K., Pozzer, A., Lammel, G., Kampf, C. J., Fushimi, A., Enami, S., Arangio, A. M., Fröhlich-Nowoisky, J., Fujitani, Y., Furuyama, A., Lakey, P. S. J., Lelieveld, J., Lucas, K., Morino, Y., Pöschl, U., Takahama, S., Takami, A., Tong, H., … Sato, K. (2017). Aerosol Health Effects from Molecular to Global Scales. *Environmental Science & Technology*, *51*(23), 13545–13567. https://doi.org/10.1021/acs.est.7b04417

Simons, A. (2016). Road transport: new life cycle inventories for fossil-fuelled passenger cars and non-exhaust emissions in ecoinvent v3. *The International Journal of Life Cycle Assessment*, *21*(9), 1299–1313. https://doi.org/10.1007/s11367-013-0642-9

Sisani, F., di Maria, F., & Cesari, D. (2022). Environmental and human health impact of different powertrain passenger cars in a life cycle perspective. A focus on health risk and oxidative potential of particulate matter components. *Science of The Total Environment*, *805*, 150171. https://doi.org/10.1016/j.scitotenv.2021.150171

Smolders, E., & Degryse, F. (2002). Fate and Effect of Zinc from Tire Debris in Soil. *Environmental Science & Technology*, *36*(17), 3706–3710. https://doi.org/10.1021/es025567p

Song, Q., & Osada, K. (2020). Seasonal variation of aerosol acidity in Nagoya, Japan and factors affecting it. *Atmospheric Environment: X*, *5*, 100062. https://doi.org/10.1016/j.aeaoa.2020.100062

Song, S., Gao, M., Xu, W., Shao, J., Shi, G., Wang, S., Wang, Y., Sun, Y., & McElroy, M. B. (2018). Fine-particle pH for Beijing winter haze as inferred from different thermodynamic equilibrium models. *Atmospheric Chemistry and Physics*, *18*(10), 7423–7438. https://doi.org/10.5194/acp-18-7423-2018

Soret, A., Guevara, M., & Baldasano, J. M. (2014). The potential impacts of electric vehicles on air quality in the urban areas of Barcelona and Madrid (Spain). *Atmospheric Environment*, *99*, 51–63. https://doi.org/10.1016/j.atmosenv.2014.09.048

Tanaka, T. Y., Orito, K., Sekiyama, T. T., Shibata, K., Chiba, M., & Tanaka, H. (2003). MASINGAR, a global tropospheric aerosol chemical transport model coupled with MRI/JMA98 GCM: Model description. *Papers in Meteorology and Geophysics*, *53*(4), 119–138. https://doi.org/10.2467/mripapers.53.119

Tessum, C. W., Hill, J. D., & Marshall, J. D. (2014). Life cycle air quality impacts of conventional and alternative light-duty transportation in the United States. *Proceedings of the National Academy of Sciences*, *111*(52), 18490–18495. https://doi.org/10.1073/pnas.1406853111

Timmers, V. R. J. H., & Achten, P. A. J. (2016). Non-exhaust PM emissions from electric vehicles. *Atmospheric Environment*, *134*, 10–17. https://doi.org/10.1016/j.atmosenv.2016.03.017

Tong, H., Arangio, A. M., Lakey, P. S. J., Berkemeier, T., Liu, F., Kampf, C. J., Brune, W. H., Pöschl, U., & Shiraiwa, M. (2016). Hydroxyl radicals from secondary organic aerosol decomposition in water. *Atmospheric Chemistry and Physics*, *16*(3), 1761–1771. https://doi.org/10.5194/acp-16-1761-2016

Valavanidis, A., Fiotakis, K., & Vlachogianni, T. (2008). Airborne Particulate Matter and Human Health: Toxicological Assessment and Importance of Size and Composition of Particles for Oxidative Damage

and Carcinogenic Mechanisms. *Journal of Environmental Science and Health, Part C*, *26*(4), 339–362. https://doi.org/10.1080/10590500802494538

Valavanidis, A., Salika, A., & Theodoropoulou, A. (2000). Generation of hydroxyl radicals by urban suspended particulate air matter. The role of iron ions. *Atmospheric Environment*, *34*(15), 2379–2386. https://doi.org/10.1016/S1352-2310(99)00435-5

Vanherle, K., Lopez-Aparicio, S., Grythe, H., Lükewille, A., Unterstaller, A., & Mayeres, I. (2021). *Transport Non-exhaust PM-emissions An overview of emission estimates, relevance, trends and policies*. Viken, Noruega: European Topic Centre on Air Pollution, Transport, Noise and Industrial Pollution (ETC/ATNI). Retrieved from https://www.eionet.europa.eu/etcs/etc-atni/products/etc-atni-reports/etc-atni-report-5-2020-transport-non-exhaust-pm-emissions-an-overview-of-emission-estimates-relevance-trends-and-policies

Vasilakos, P., Russell, A., Weber, R., & Nenes, A. (2018). Understanding nitrate formation in a world with less sulfate. *Atmospheric Chemistry and Physics*, *18*(17), 12765–12775. https://doi.org/10.5194/acp-18-12765-2018

Wallenborn, J. G., McGee, J. K., Schladweiler, M. C., Ledbetter, A. D., & Kodavanti, U. P. (2007). Systemic Translocation of Particulate Matter-Associated Metals Following a Single Intratracheal Instillation in Rats. *Toxicological Sciences*, *98*(1), 231–239. https://doi.org/10.1093/toxsci/kfm088

Weibull, W. (1951). A Statistical Distribution Function of Wide Applicability. *Journal of Applied Mechanics*, *18*, 293–297.

Wong, J. P. S., Yang, Y., Fang, T., Mulholland, J. A., Russell, A. G., Ebelt, S., Nenes, A., & Weber, R. J. (2020). Fine Particle Iron in Soils and Road Dust Is Modulated by Coal-Fired Power Plant Sulfur. *Environmental Science & Technology*, *54*(12), 7088–7096. https://doi.org/10.1021/acs.est.0c00483

Wu, W., Bromberg, P. A., & Samet, J. M. (2013). Zinc ions as effectors of environmental oxidative lung injury. *Free Radical Biology and Medicine*, *65*, 57–69. https://doi.org/10.1016/j.freeradbiomed.2013.05.048

Xiong, Q., Yu, H., Wang, R., Wei, J., & Verma, V. (2017). Rethinking Dithiothreitol-Based Particulate Matter Oxidative Potential: Measuring Dithiothreitol Consumption versus Reactive Oxygen Species Generation. *Environmental Science & Technology*, *51*(11), 6507–6514. https://doi.org/10.1021/acs.est.7b01272

Xu, J., Chen, J., Zhao, N., Wang, G., Yu, G., Li, H., Huo, J., Lin, Y., Fu, Q., Guo, H., Deng, C., Lee, S.-H., Chen, J., & Huang, K. (2020). Importance of gas-particle partitioning of ammonia in haze formation in the rural agricultural environment. *Atmospheric Chemistry and Physics*, *20*(12), 7259–7269. https://doi.org/10.5194/acp-20-7259-2020

Yang, Y., & Weber, R. J. (2022). Ultrafiltration to characterize PM2.5 water-soluble iron and its sources in an urban environment. *Atmospheric Environment*, *286*, 119246. https://doi.org/10.1016/j.atmosenv.2022.119246

Yu, H., Wei, J., Cheng, Y., Subedi, K., & Verma, V. (2018). Synergistic and Antagonistic Interactions among the Particulate Matter Components in Generating Reactive Oxygen Species Based on the Dithiothreitol Assay. *Environmental Science & Technology*, *52*(4), 2261–2270. https://doi.org/10.1021/acs.est.7b04261

Yumimoto, K., Tanaka, T. Y., Oshima, N., & Maki, T. (2017). JRAero: the Japanese Reanalysis for Aerosol v1.0. *Geoscientific Model Development*, *10*(9), 3225–3253. https://doi.org/10.5194/gmd-10-3225-2017

Zhao, J., & Wang, J. (2016). Integrated Model Predictive Control of Hybrid Electric Vehicles Coupled With Aftertreatment Systems. *IEEE Transactions on Vehicular Technology*, *65*(3), 1199–1211. https://doi.org/10.1109/TVT.2015.2405918

Zhou, Y., Huang, X. H., Bian, Q., Griffith, S. M., Louie, P. K. K., & Yu, J. Z. (2015). Sources and atmospheric processes impacting oxalate at a suburban coastal site in Hong Kong: Insights inferred from 1 year hourly measurements. *Journal of Geophysical Research: Atmospheres*, *120*(18), 9772–9788. https://doi.org/10.1002/2015JD023531